Final Report for

# STUDIES OF THE STRUCTURE OF THE IONOSPHERE

Contract No. NASw-342

Prepared by

Lockheed Palo Alto Research Laboratories
3251 Hanover Street
Palo Alto, California

for

National Aeronautics and Space Administration
400 Maryland Avenue, S.W.
Washington, D. C.

Abstract

16077

This contract, Studies of the Structure of the Ionosphere, was established to study the ionospheric profile up to 1000 km with an ion trap and two mass spectrometers flown in a Javelin sounding rocket. The quadrupole ion mass spectrometer required flight testing and this was accomplished by flying it and an ion trap in a Nike-Apache rocket preliminary to the more expensive Javelin flight. The nose cone of the first Nike-Apache failed to eject so a second Nike-Apache flight was added to the program. From the second flight ion concentration and valuable ion temperature data were obtained. The latter data showed unexpected temperature stratification in the E- and lower F-regions at midday with peak-to-valley temperature differences of several hundred degrees.

The Javelin rocket containing an ion trap, a quadrupole ion mass spectrometer, and a magnetic light ion mass spectrometer was flown near local midnight on July 7, 1964. Ion concentration and temperature profiles were obtained from the ion trap and an ion composition (mass range 12-48 amu) profile was obtained from the quadrupole mass spectrometer. Unexpected rocket motions rendered analysis difficult, but the results are nevertheless meaningful.

Author

Table of Contents

List of Figures and Illustrations

# STUDIES OF THE STRUCTURE OF THE IONOSPHERE

## INTRODUCTION

### Goals

The main purpose of this program was to study the ionospheric structure by measuring profiles of various ionospheric parameters from a single high altitude sounding rocket, the Javelin rocket. The information obtained would hopefully contribute to our understanding of the complex phenomena which occur in the F-region of the ionosphere. One of the instruments to be flown in the Javelin rocket required flight testing in a lower altitude (and hence less expensive) rocket. Thus, the program included a Nike-Apache flight of instruments similar to those intended for the Javelin flight. The structure of the ionosphere was to be studied by making simultaneous measurements of the total ion concentration, the relative composition of the ions from 1 amu to 48 amu, and the average kinetic energy (or temperature) of the ions. To accomplish this the Javelin rocket was provided with a payload which included an ion energy analyzer (Ion Trap), a Paul-type quadrupole ion mass spectrometer to operate over the range of 12 to 48 amu, and a magnetic-type light ion mass spectrometer to operate in the range 1 to 16 amu. With this spectrometer payload it was expected that the altitude at which $He^+$ ions predominate, and the altitude at which $H^+$ ions finally predominate in the ionosphere could be easily obtained in addition to the other objectives of the mission. To help insure being able to detect these diffusively separated layers the Javelin flight was conducted at night when these light ion layers are expected to be lowest in altitude.

## Flight Schedule

The first effort to flight test the quadrupole spectrometer in a Nike-Apache (14.30) payload was attempted 23 August 1962 but was unsuccessful presumably due to failure of the rocket nose cone to properly eject and expose the instruments to the ionosphere. A second Nike-Apache (14.110) payload, identical with the first except for an improved nose-cone separation technique, was flown from Wallops Island on 8 May 1963. Not all of the flight objectives were met because the quadrupole spectrometer failed to produce ion peaks. However, a large coning angle seemed evident from the telemetry records which, with severe entrance angle limitations and somewhat low sensitivity in the spectrometer, could account for the lack of data. The ion trap, with a wide acceptance angle, obtained valuable and interesting data. The culmination of this program came with the successful flight of the Javelin 8.03 payload on 7 October 1964 from Wallops Island, Virginia. Although the telemetry record gives strong evidence for a larger rocket coning angle than expected, valuable data were obtained from the quadrupole ion mass spectrometer and from the ion trap. The magnetic light ion mass spectrometer failed to operate, presumably as a result of a component failure in the device. Even without the light ion mass spectrometer the Javelin flight must be considered a success from the data that were obtained.

## Results

The general results of this program are that an ion concentration and temperature profile has been obtained between 100 and 160 km, the temperature profile showing the unusual behavior of a wave-like structure superimposed upon the expected gradual increase with altitude which suggests temperature

stratification at midday. Further, an ion concentration and ion temperature profile from 260 to 1000 km has been obtained near midnight. At the same time, the major "heavy" ion constituent profiles have been measured in the same altitude region.

## NIKE-APACHE 14.30

### Flight Information

The Nike-Apache 14.30 sounding rocket was fired from Wallops Island, Virginia, 23 August 1962 at 1710 UT. The scientific instruments included in this payload were a quadrupole ion mass spectrometer and a hemispherical ion energy analyzer. The payload section from this rocket is shown in Figure 1. The two scientific instruments are mounted near the top of the payload section so that they may be located in the ram position of the rocket during the flight (their entrance faces are covered in the figure). The ion energy analyzer is shown on the left and the quadrupole mass spectrometer is shown on the right of the payload in the figure. Below these two instruments are located the battery pack, power converters and telemetry system used for this flight. The tubing running along the left side of the payload is part of a dry nitrogen flush system to keep the mass spectrometer clean and free from contamination. For flight a tubular cover section fits over the payload section with an ejectable nose cone to expose the scientific instruments to the ambient ionosphere. On the bottom part of the payload can be seen a set of dark cylindrical insulators into which were screwed the turnstile antenna for the telemetry system and a set of smaller metallic cylinders which served as exhaust vents for the payload section during rocket ascent before the nose cone is removed.

Results

The objectives of this flight were: (1) to provide in-flight testing of the quadrupole mass spectrometer, (2) to measure the ambient ion composition with altitude, and (3) to measure the ambient ion concentration and temperature with altitude. Unfortunately, none of these objectives were satisfactorily accomplished due, apparently, to the failure of the nose cone to eject and expose the scientific instruments. No telltale signal to indicate positive nose separation was provided on this flight so it is not possible to be absolutely certain of what happened to the nose cone. The sensitive electrometers of both the ion trap and the mass spectrometer indicated positive firing of the nose cone pyrotechnics, but no ion signals were observed in either instrument. Since power was definitely applied to both scientific instruments, as indicated by the sweep outputs on the telemetry, and since computation showed that an ion current should have been observed in the ion energy analyzer regardless of vehicle orientation, it seems logical to conclude that the nose cone failed to separate from the payload.

It could be noted in passing that the Nike-Apache rocket performance on this flight was far from satisfactory, apogee being only 129 km instead of the predicted 168 km. However, it is quite unlikely that this could have completely accounted for the failure to obtain usable scientific data.

## NIKE-APACHE 14.110

Flight Information

The Nike-Apache 14.110 sounding rocket was fired from Wallops Island, Virginia, 8 May 1963, at 1723 UT. The scientific payload for this rocket was the same as for the Nike-Apache 14.30 described in the previous section.

Figure 1 also applies to the 14.110 payload. The only significant change in this rocket was the inclusion of an improved nose cone separation scheme and a telltale signal to verify nose cone separation.

## Results

The scientific objectives of this flight remained the same as for the unsuccessful 14.30 flight. These objectives were only partially met, but yet very valuable scientific data were obtained from this flight. The rocket performed satisfactorily carrying the payload to a peak altitude of 167 km. The nose cone release mechanism operated and positive indication of nose separation was obtained from the telltale designed for that purpose. Very useful and valuable data were obtained from the ion energy analyzer the results of which will follow. However, no mass composition information was obtained. From all available indication the quadrupole mass spectrometer was working electrically, but no mass peaks were observed from it. Since it was exposed to the ionosphere and since it appeared to be working electrically, we concluded that the durrent sensitivity was too low and the usable entrance cone too small for the angle of attack of the rocket. Such a conclusion is only a presumption since there were no orientation sensors on this rocket.

## Ion Trap Analysis and Interpretation

### Instrument

The significant scientific results obtained from this flight have been reported in detail in the scientific literature (Knudsen and Sharp, 1965) so only a brief discussion will be given here. The construction of the ion trap is illustrated schematically in Figure 2. The principle of operation is

the same as that of planar ion traps reported elsewhere (Pearse, 1962; Hanson and McKibben, 1961). The construction is unique in that the usual plane geometry of the grids and collector plate has been replaced by a hemispherical geometry. With this hemispherical grid construction, the shape of the ion current versus retarding potential curve is not changed by a change in the angle of attack $\kappa$ when the trap is traveling through the plasma with a velocity large compared with the thermal velocities of the ions. The amplitude of the curve is altered by a change in $\kappa$ because of the change in the effective area of the aperture, but the geometry of the electric field seen by the ions is not changed. The suppressor grid and collector were maintained respectively at -4 and 0 volts relative to the rocket body through the flight.

Data

A typical interval of data obtained from the flight is illustrated by Figure 3. The retarding potential and three ion current traces are shown as a function of time. The retarding potential was swept from +4.5 to -0.5 and back to 4.5 volts approximately every two seconds. Thus, temperature was measured at approximately one-second intervals. Near 100 km the corresponding altitude spacing was one kilometer.

The behavior of the ion current with retarding potential can be understood as follows. Ions enter the surface grid with a mean energy $eV_m$, but with individual energies distributed about this mean value consistent with the local ionic temperature. With the retarding potential at a large positive potential relative to $V_m$, an insignificant number of ions have sufficient energy to reach the collector. As the retarding potential decreases, the number of particles with sufficient energy to reach the collector

increases until all ions are collected. Further decrease in the retarding potential does not increase the ion current.

The actual behavior of the ion current as illustrated in Figure 3 contains instrumental additions. Systematic electronic noise occurred rather continuously throughout the flight independently of the state of the retarding potential. The period of this noise was just half that of the roll rate of the rocket and was assumed to be electronic in origin. During the interval of the retarding potential cycle when the ion current is not expected to vary, a definite modulation of the ion current can be observed. The fundamental frequency of the modulation has the same period as the electronic noise. The amplitude of the modulation varied slowly throughout the flight, decreasing from 10% of the mean ion current near 100 kilometers to approximately 5% at 160 km. Our explanation for the ion current modulation is that the angle of attack of the rocket was not zero and as the rocket rotated about its symmetry axis the ion current to the collector was modulated by small geometrical changes in the transmission of the grids. Modulation of this type would increase with increase in angle of attack when the vehicle was moving reasonably fast relative to the thermal velocity of the particles.

In addition to the preceding disturbances, a shallow depression can be seen in the ion current centered on the lower turning point of the retarding potential trace. This behavior occurred consistently and cannot be attributed to imperfections in the electronic apparatus; it is believed to be caused by a decrease in the effective transmission coefficient of the retarding potential grid as the potential is decreased. With the grid positive, the ions would tend to be repelled from the wires toward the center of the grid openings;

with the grid negative the ions would be attracted toward the wires. A decrease in transmission of 10% can be understood in this manner and is the approximate decrease observed.

Data Analysis

After digitization of the analog signals at a rate of 312 points per sec, the data were numerically processed as follows. A time interval, $\Delta t_1$ (see Figure 3), centered on the upper turning point of the retarding potential trace and equal to the period $\tau$ of the systematic electronic noise was Fourier analyzed to determine the coefficients of the harmonics up to the fourteenth. The signal reconstructed from these harmonics was then subtracted from the time intervals $\Delta t_2 (= 0.3$ sec) and $\Delta t_3$ $(= 2\tau)$. By this process the systematic electronic noise was removed from the two time intervals.

The ion current telemetry voltage behavior during time interval $\Delta t_3$ was then assumed to be of the form

$$I(t) = I_o[1 + g(t - t_o)]\ TR(r) + R(t) \qquad (1)$$

where $I(t)$ is the total ion current; $I_o[1 + g(t - t_o)]$ is a linear variation resulting from temporal change in rocket velocity, spatial change in ion concentration, and/or change in angle of attack; $TR(t)$ is the periodic transmission coefficient; $R(t)$ is a random noise component introduced by the telemetry channel; $t$ is the time; and $t_o$ is the time of the lower retarding potential turning point. $TR(t)$ and $R(t)$ are assumed to have the properties

$$TR(t + \tau) = TR(t)$$

$$\max TR(t) = 1.0$$

$$\int_{t_2}^{t_2 + \delta} R(t)\, dt = 0$$

where $\tau$ is the common period of both the systematic electronic noise and ion current modulation, and $\delta$ is a small fraction of $\tau$. By appropriate analysis of $I(t)$ within the interval $\Delta t_3$, the parameters $I_o$, $g$, and $TR(t)$ were then determined, and $I(t)$, within the time interval $\Delta t_2$, was corrected using the following formula:

$$I^*(t) = \frac{I(t)[1 + g(t_m - t_o)]}{TR(t)[1 + g(t - t_o)]}$$

where $I^*(t)$ is the corrected ion current, and $t_m$ is the time corresponding to the middle of the interval $\Delta t_2$.

In this way changes in the ion current during interval $\Delta t_2$ resulting from systematic electronic noise, modulation, and changes in the ambient ion concentration and angle of attack were removed. The ion current within time interval $\Delta t_4$ was corrected in an analogous way. Any linear trend in the data ($g \neq 0$) was removed only when $g$ was significant as determined by the statistics of the data.

Random noise corresponding to $R(t)$ introduced into the retarding potential telemetry signal was removed in analysis by fitting a straight line into the observed signal by the least squares technique.

The procedure described above resulted in a set of data consisting of 94 pairs of corrected and correlated ion current and retarding potential values for each sweep of the retarding potential between its limits. The temperature, ion concentration, and rocket potential were determined for each set of data by selecting the values of these parameters which minimized the sum of the squares of the deviations of the experimental ion current data from the theoretically computed value. Simultaneously, confidence limits for the parameters were inferred from the distribution of the experimental data about the theoretical curve. The numerical techniques used in accomplishing these analyses are described by Moore and Zeigler (1960) and McWilliams (1963).

The theoretical expression for the ion current used in the analysis is

$$I = e\, A \cos \kappa \frac{2}{\sqrt{\pi}} N v \alpha \xi(a,b) \qquad (2)$$

where

$$\xi(a,b) = 1/4 \exp\left[-(b - a)^2\right] \cdot \left\{\frac{b}{a} + 1 + \frac{1}{2a^2}\left[\exp(-2ab) - 1\right]\right\} + \frac{\sqrt{\pi}}{4} a\left[1 - \operatorname{erf}(b - a)\right]$$

$$a = v/\alpha$$

$$b = \frac{\left[2e(V + S)/M\right]}{\alpha}$$

$$\alpha = (2kT/M)^{1/2}$$

e is the electronic charge, A is the effective area of the ion trap aperture, $\kappa$ is the angle of attack, N is the ion number density, v is the rocket velocity,

V is the retarding potential relative to the rocket potential, S is the rocket potential relative to the plasma potential, M is the ionic mass, k is the Boltzmann constant, T is the temperature, $\alpha$ is the most probable ion velocity, a is the dimensionless vehicle velocity in units of $\alpha$, and b is the dimensionless velocity of an ion in units of $\alpha$ with just sufficient energy to overcome the retarding potential.

An example of the fit of Equation 2 to one set of data is illustrated in Figure 4. The only significant systematic deviation of the data from the theoretical curve is the shallow depression in the ion current at low retarding potential. As has been pointed out, this depression occurs consistently and probably results from changes in transparency of the retarding potential grid with retarding potential.

Results

The ion temperature determined by the least squares analysis is illustrated in Figure 5. Each temperature value was computed from one set of data. The temperature values for all sets of data between the height interval 100 to 160 km are indicated, with one exception. The error bars indicate confidence intervals assigned to the individual temperature points in the manner described by Moore and Zeigler (1960). They are not absolute error limits. The three neutral temperature curves indicate the temperature predicted from models by Harris and Priester (1962), Anderson and Francis (1964) and Nicolet (1962). The curves by Harris and Priester and Anderson and Francis are appropriate for a 10.7-cm solar flux value of 86 (in units of $10^{-22}$ watt $m^{-2}$ sec) and a local time of 1300. The curve by Nicolet was chosen to have an isothermal temperature at high altitude of $1180^{\circ}K$, which is that attained by the Anderson and Francis curve.

The experimental temperature profile has been drawn through the mean of successive temperature values in the intervals where the values alternated in amplitude as has been justified previously. The large amplitude alternations in the data just above 100 km occur in the altitude region where N is increasing most rapidly with height and S is decreasing most rapidly with height. Both of these time changes affect the derived temperature in the same sense and the high and low values are properly phased with the retarding potential - the high values occurring when the retarding potential was increasing. Since the time rate of change of N was approximately removed from the data before least squares analysis, the alternations are most likely caused by a large negative value of dS/dt. The values of S derived by least squares with the assumption that it was constant varied smoothly from -1.6 at 99 km to -1.9 at 105 km to -2.0 at 160 km. These values illustrate that the fastest decrease of S did occur at the 100-km level; however, the value of dS/dt computed from these data would produce temperature alternations of $\pm$ 10% only.

Above 120 km the trend of the experimental temperature profile parallels the predicted neutral temperature profiles rather satisfactorily but may be systematically high. Superimposed on this trend is a wave-like variation with a peak-to-trough amplitude of approximately 200$^{\circ}$K and a wavelength of approximately 12 km. At 110 km, the temperature is approximately twice the model temperature and increases downward.

The temperature variations indicated by the data are unexpected. Nevertheless after ruling out possible experimental and data processing sources of such variation, we have concluded that the variations are real. Before the processing of the data described here, the electronic noise and

current modulation were removed from the original data in a different and somewhat less objective manner than that reported here. No correction for time variations in I resulting from time variations in N and K was made. This first analysis, reported orally (Knudsen and Sharp, 1963), yielded essentially the same variations as those reported here. The refined analysis only reduced the magnitude of the thermal peaks. Consequently, our method of data processing does not appear to be the source of the temperature structure. Time rate of changes of N, K, and S are ruled out because steady changes in these values are discernible as temperature alterations, and it would require an improbable sequence of alterations in sign or magnitude of these rates to produce the sequence of values defining the peaks and troughs.

Because of the rather uniform spacing of the peaks and troughs, it is tempting to look for an explanation in terms of rocket precession. Regular changes in angle of attack could result from the axis of precession making a significant angle with the velocity vector of the rocket center of gravity. A precession explanation for the peaks and troughs has been ruled out for the following reasons. If the angle of attack of the rocket were periodically to exceed $45^{\circ}$ by a significant amount, the computed temperature would also be expected to vary, since the first-order correction term to Equation 2 which influences the shape of the ion current versus retarding potential curve was not used in the analysis. We emphasize that the angle of attack would need to exceed $45^{\circ}$ by a significant amount because the temperature computed by means of Equation 2 with first-order correction included varied less than 0.2% for assumed angles of attack from 0 to $45^{\circ}$ for sets of experimental data at 104- and 134-km altitude. The temperature variation

illustrated in Figure 4 in this altitude range is ± 20%. Correlated with the spurious temperature changes resulting from failure to correct for angle of attack would be spurious changes in computed ion concentration, for the amplitude of the ion current is proportional to the cosine of the angle of attack (see Equation 2). Suppose, for example, that the angle of attack were periodically varying from 40 to 60°. The cosine of the angle would change from 0.77 to 0.50 and would change the computed concentration, for example, from approximately $3 \times 10^5$ to $2 \times 10^5$ $cm^{-3}$, a very obvious change. No such ion concentration changes correlated with the temperature changes are observed. In addition to this evidence, the time intervals between temperature peaks are not uniform. The intervals are 17.3, 14.7, and 25.3 seconds. The intervals would be regular in time if produced by precession. These intervals of time are also not consistent with other internal evidence. The time variation of the ion current modulation noise amplitude which we have assumed to increase with increase in angle of attack suggested that a small change in angle of attack was occurring with a period of approximately 61 seconds.

Horizontal winds exist in the lower E region which may have velocities approaching 200 m/sec and which have considerable vertical structure. Winds of this magnitude could deviate the angle of attack through 11°. Again, for such a change to produce the computed temperature variations, the angle of attack in the absence of the wind would have to exceed 45°. An increase in angle of attack of 10° from a steady value, of, say 50° would produce an apparent change in concentration of 25% and would be observable in the concentration profile.

The height variation of the measured ion concentration is illustrated in Figure 6. The ion concentration has been multiplied by 1.6 to bring the concentration maximum near 108-km altitude into agreement with the concentration corresponding to the E-layer critical frequency observed on a concurrently recorded ionogram. The angle whose cosine is 1/1.6 is 51° and compares favorably with a half-cone precession angle of 47°, which is to be expected if the precession period were, in fact, 61 seconds. However, the laboratory calibration of the ion trap transmission could be in error by the factor 1.6. What little experimental evidence exists suggests that the precession angle was approximately 50°, and that the axis of precession was approximately parallel to the flight trajectory. A further complication in interpreting the concentration results is the lack of a quantitative theory to describe the behavior of the ion trap in the transition region between the free molecular flow and continuum flow regions. The neutral particle concentration in front of the rocket is larger than the ambient concentration within the transition region. How the ion concentration is affected is unknown.

The electron concentration profile deduced from the concurrently recorded ionogram is also illustrated in Figure 6. The height of the ionosonde profile is seen to be too large by approximately 4 km. Positive height errors of this magnitude are to be expected when the electron density gradient at the starting height cannot be inferred from the ionogram, as was true with the ionogram in question (J. W. Wright, private communication). When the ionosonde profile is lowered by 4 km, it agrees with the ion density profile satisfactorily up to a height of approximately 140 km, where the ion-trap-derived ion concentration progressively becomes larger than the

ionosonde electron concentrations. We suppose that this departure is caused by enhanced ion concentration near the rocket as the rocket velocity decreases near the top of the trajectory.

The ion concentration data are presented primarily to illustrate the lack of any prominent concentration features which correlate with the thermal structure. A relatively narrow and small amplitude maximum does appear to occur at the same height as the thermal peak at 116 km. The only other ion concentration manifestation of the thermal peaks which suggests itself is an enhanced rate of increase of ion concentration with height on the bottom side of the peak and a diminished rate of increase above.

After investigating possible instrumental and data processing effects as the cause of the observed wave-like temperature variations, it does not seem reasonable to assign the variation to these effects. Since rocket attitude was not measured during the flight, rocket precession becomes suspect. Rocket precession has been ruled out as a plausible explanation for the following reasons. The shape of the ion current versus retarding potential curves from which the temperature is computed is insensitive to the angle of attack for angles at least as large as $45^{\circ}$. On the other hand, the amplitude of the curve depends directly on the cosine of the angle of attack. Variations in angle of attack sufficient to produce significant changes in the computed temperature would produce significant variations in the computed ion concentration. The variations in ion concentration would be correlated with the temperature variations. No obvious correlation is observed. In addition to this evidence, the time intervals between temperature peaks are not equal.

The data are uncorrected for changes in the transmission factor of the retarding potential grid with changes in retarding potential. This effect is estimated to introduce a systematic, positive error in the data of the order of 10%.

The observed increase in temperature below 115 km can be explained qualitatively as arising from aerodynamic heating of the ions in the transition flow region. However, this increase may, in part, be a real effect.

An attractive mechanism for producing the observed wave-like temperature variation is internal atmospheric gravity waves. The observed temperature variations are consistent with those expected from a gravity wave producing a horizontal wind velocity of 150 m/sec. The vertical wavelength of the temperature variations is smaller, however, than that believed possible for gravity waves in the altitude interval of interest in this paper.

If it is assumed that the measured temperature profile is representative of a quasi-steady state daytime profile with conduction the dominant heat transfer mechanism, then the temperature troughs must be maintained by radiation loss, and the heat input required to maintain all of the thermal peaks is at least four times the total estimated energy in the solar extreme ultraviolet.

The possibility that the atmosphere may not be in hydrostatic equilibrium in the lower E region raises serious questions as to the adequacy of attempting to determine detailed temperature profiles from measurements of density or pressure singly.

The retarding potential analyzer is a potentially valuable instrument for extending atmospheric temperature measurements into the important height range 100-160 km.

JAVELIN 8.03

Flight Information

The experimental work on this contract was culminated by the flight of the Javelin 8.03 rocket and payload on October 7, 1964 at 2352 LT (0352, October 8, UT) from Wallops Island, Virginia. The payload rose to a peak altitude of 1155 km with the nose cone being ejected at the appointed time, exposing the scientific instruments to the ionosphere from about 265 km altitude. Strong telemetry signals were received throughout the flight and there was continuous skin tracking of the vehicle from T + 9.15 to T + 1091 seconds. From the tracking information the Javelin rocket seemed to perform very satisfactorily. However, information from the scientific instruments indicate that the fourth stage rocket-payload combination assumed an unusual orientation. The telemetry station AGC record showed a smooth rocket spin rate of nearly 10 cps prior to nose separating but this spin rate decreased to about 1.5 cps after separation and there were peculiar modulation effects on the AGC record in addition. This is a good indication that the rocket was performing in an unexpected manner after separation.

The scientific objectives of this flight were to obtain total ion density, ion composition and ion temperature profiles for the night ionosphere over Wallops Island. Of particular interest was the location of the altitude where light (1-40 amu) ions become more predominate than the heavy ions (>12 amu). These objectives were to be met in this payload by the inclusion of a heavy ion (12-48 amu) mass spectrometer, a light ion (1-16 amu) ion mass spectrometer, and an ion trap operated as a retarding potential analyzer.

The payload also contained an eleven (11) channel FM/FM telemetry system, power converters and batteries, but, unfortunately, did not contain any mechanism for detecting rocket orientation.

Figure 7 is a photograph of the completed payload. At the top is the flat plate which serves as a ground plane for the entrance apertures of the three scientific instruments. The lower left instrument is the quadrupole mass spectrometer, the upper center instrument is the light ion mass spectrometer, and the right instrument is the hemispherical ion trap. All entrance grids, apertures, the aperture plate and, in fact, all parts of the structure above the extension ring shown were gold plated to eliminate contact potential differences. Figure 8 shows the payload section attached to the fourth stage motor (the way it would be in flight) mounted ready for spin balancing. The attachment at the top is the spring and push-plate used for ejecting the fibreglass nose cone. Movement of the pressure-plate away from the aperture plate triggered a signal which indicated positive nose cone separation.

Not all of the scientific objectives of this flight were accomplished since the light ion mass spectrometer failed to provide any scientific information. This failure resulted from a component defect in the spectrometer itself. The other two instruments worked well and the analysis of their data will follow in a later section.

## Instrument Descriptions

The ion trap flown in this package was identical to that flown in the Nike-Apache 14.110 package. Figure 2 is a schematic representation of it and the description in the Nike-Apache 14.110 section of this report applies to the Javelin 8.03 instrument.

Since the light Ion Mass Spectrometer failed to provide any useful scientific data only a brief description of it will be given. The analyzing section of this instrument was a $90^{\circ}$ magnetic sector. A first order focusing correction was accomplished by locating the center of the analyzing entrance aperture, the center of the exit aperture and the center of curvature for the magnetic sector on the same straight line. As shown in Figure 7, the instrument entrance aperture was a fine-mesh screen-covered orfice electrically attached to the vehicle ground. Directly behind this aperture was the entrance to the analyzing section. The entire analyzing section was swept linearly from -700 V to +20 Volts dc to focus $H^+$, $He^+$ and $O^+$ ions, respectively.

The ion detector used was a small Bendix magnetic electron multiplier. It was used as a current amplifier and its output was fed into a conventional automatic ranged electrometer. This instrument had a dynamic range of $10^6$, covered in eight (8) distinct ranges, and was sufficiently sensitive to be able to detect ion concentrations as low as $\approx 3/cm^3$. Telemetry information from the flight showed the sweep operating properly, and transient noises did trigger the electrometer and ranging circuits once, showing their proper operation. This evidence suggests that the Bendix multiplier was not working. This failure could be caused by the high voltage power supply for the multiplier failing, a key lead wire becoming disconnected or breaking, or the actual multiplier failing during powered flight. It is not clear which of these explanations should be invoked to account for this lack of data.

A description of the operation of the quadrupole ion mass spectrometer will be given here so that understanding of the data analysis will be facilitated later. This device utilizes a quadrupole electrodynamic field with both RF and dc potentials being applied. The use of this system as a mass spectrometer was first proposed by W. Paul and the detailed theory of its operation has been given by Paul, et al. (1958). Considerable detailed investigation of the characteristics of the quadrupole mass spectrometer has been conducted by W. Brubaker (1961).

The ideal hyperbolic pole pieces were approximated in our instrument by using cylindrical rods. The four rods, 1 cm in diameter and 15 cm long, were mounted parallel to each other and symmetrically spaced so that the surface of each rod was

$$\frac{1}{1.16} \times \text{rod radius} = 0.431 \text{ cm}$$

from the center of symmetry. Opposite pairs of rods are connected together electrically and the rod system is driven by an RF-oscillator with a dc potential difference applied between the pairs of rods.

Ions enter the mass spectrometer through the grounded screen of the entrance aperture and are accelerated toward the rod system by a -20 Vdc potential applied to a second grid. Passing through this second grid the ions travel through a drift tube-lens combination and are injected into the quadrupole field of the rod system. Ions which are injected on-axis with negligible transverse velocity components and which have the correct charge to mass ratio for the quadrupole field applied travel the length of the rod system along bound paths and are available to be collected as ion current

at the opposite end of the rod system. All ions with other than the correct charge-to-mass ratio follow unbound trajectories and are collected by the rods themselves or on the inner walls of the spectrometer container.

The equations of motion of a particle in the quadrupole field are Mathieu equations and their solution can best be described by a stability diagram which shows regions where the particle motion is stable and regions where it is unstable. Stability diagrams are generally given in an a-q plane where

$$a = \frac{8eV_{dc}}{Mr_o^2\omega^2} \tag{3}$$

and

$$q = \frac{4eV_{RF}}{Mr_o^2\omega^2} \tag{4}$$

where e is the electronic charge, M is the mass of the ion, $\omega$ is the angular frequency of the applied RF-field, $r_o$ is $\frac{1}{1.16}$ x rod diameter, $V_{dc}$ is the dc voltage applied to the rods, and $V_{RF}$ is the amplitude of the RF voltage applied to the rods. In the absence of a dc field, i.e. a=o, ions are stable for q between zero and 0.92. Thus, for a given applied RF voltage all masses greater than a certain one (determined by using q = 0.92, $V_{RF}$, $r_o$ and $\omega$ in equation 4) have stable paths and can be collected as current. Application of a dc-potential limits the range of masses which have stable paths. Thus, the mass resolution is determined by the application of dc-fields. In fact, by making the dc-field large enough, for a given RF-field, the spectrometer will go into cut off and collect no ions at the exit of the rod system.

With this instrument a mass spectrum is swept by first establishing a ratio of $V_{dc}/V_{RF}$ which will provide the desired mass resolution then sweeping the applied voltages over a range appropriate for the mass range of interest,

keeping the $V_{dc}/V_{RF}$ ratio always constant. For any good resolution the stability diagram gives an average q-value of 0.706. Thus, the expression for determining which mass will be permitted to pass through the rod system is, from Equation 4,

$$M = \left(\frac{4e}{0.706 r_o^2}\right) \frac{V_{RF}}{\omega^2} . \qquad (5)$$

For the instrument flown in the Javelin 8.03 package $r_o$ = 0.431 cm and f = 2 megacycles/sec. Thus, the 12-48 amu mass range was covered by applying a sweeping RF voltage from 65 to 255 volts peak. In these calculations and in the flight data it is assumed that all ions analyzed are singly charged.

The analyzed ions were collected at the end of the analyzer system in a Faraday cup which was carefully shielded from the analyzer fields. This current was converted to a voltage by an automatic ranged electrometer - ac-amplifier combination which had a combined current sensitivity of $3 \times 10^{-12}$ amp/volt on its most sensitive range. There were four ranges, each a factor of $\sqrt{10}$ different in sensitivity from adjacent ranges.

The voltage sweep applied to the rods was a symmetrical triangle of period 1.95 sec. This meant that a complete mass spectrum was obtained every 0.975 sec. A master clock triggered a master dc-sweep which provided the changing dc-voltage to the rods and was also used to drive the RF oscillator. A part of the RF signal was rectified and compared to the applied dc-voltage to keep the $V_{dc}/V_{RF}$ ratio fixed. To assure proper resolution coverage the $V_{dc}/V_{RF}$ ratio was changed every sweep period through a series of four resolution settings. One setting had a poor resolution, another was near cut-off and there were two settings near the optimum resolution value of 20 near mass 20 so that adjacent mass peaks could be separated. Operation of this device in flight has shown that such a variable resolution system is not needed.

The resolution can easily be established in the laboratory and be expected to remain the same in flight.

## Ion Trap Analysis and Interpretation

The construction of the ion trap is illustrated in Figure 2. It was mounted on the nose plate of the rocket with trap axis parallel to but displaced from the spin axis. The use of hemispherical grids and collector plate has the virtue of making the shape of the ion current vs retarding potential curve relatively insensitive to the angle of attack provided the latter is not large and remains constant during the sweep period. The surface grid and collector were operated at rocket potential, and the suppressor grid, at -4.0 volts.

A representative interval of data is illustrated in Figure 9. The retarding potential was swept between -0.7 and 4.0 volts with a cycle time of 1.63 seconds. One characteristic curve was obtained every 0.8 seconds. Because the rocket motion was unfavorable, the ion current remained on the most sensitive scale (x 25) throughout the flight. On this scale a displacement current produced by the changing voltage on the retarding potential grid may be observed. Because the time rate of change of the retarding potential is constant during the recording of one characteristic curve, the displacement current is constant and introduces no distortion into the curve - only a displacement.

### Data Analysis

The x 25 ion current analog signal was digitized and processed numerically. To remove the small distortion introduced by two RC coupled amplification stages, the digitized signal was inverted. The equation for accomplishing the inversion through one RC coupled stage is

$$V(T) - V(t_o) = V'(t) - V'(t_o) + \frac{1}{RC} \int_{t_o}^{t} V'(\tau)\, d\tau \qquad (6)$$

where V is the signal prior to passing through an RC network, and V', the signal after passing through the network. The signal was operated on twice by the inversion program to remove the effect of the two stages of amplification.

The amplitude of each characteristics curve was computed by taking the difference in signal level when the sweep voltage was near -0.7 and 4.0 volts. The two amplitude values common to the same -0.7 volt turning point of the retarding potential were averaged and are plotted in Figure 10 as a function of system time in seconds. Similarly, the time derivative (dI/dt) of the amplitude at the same turning points were determined and are plotted on Figure 10. System time is measured from 0000 hrs. (EDST), Oct. 7, 1964. Apogee occurred at 86508 seconds (0002 hrs., EDST, October 8, 1964) which is approximately 2300 hrs. local time. The rocket passed through the F2 peak at approximately 86070 and 86936 seconds.

The amplitude and slope are computed from that position of the characteristic curve for which the retarding potential is less than zero. In this interval no ions are being retarded. The amplitude is seen to have a periodic variation with period of approximately 12.8 seconds with perhaps a smaller, shorter period variation superposed. We shall not consider the smaller variation. The large periodic variation is most pronounced at the lower altitudes at which time the rocket velocity is approximately three times the ion thermal velocity. The time derivative is also seen to have

this same period. The phasing of the time derivative is such that the maximum of the time derivative occurs when the amplitude of the ion current is decreasing and is at its running average. This behavior is discussed further hereafter.

The running average signal levels near 300 km altitude on both the up and down leg of the flight are of approximately the same magnitude and are both approximately a factor of ten smaller than expected had the angle of attack of the rocket been close to zero during either portion of the flight. The signal levels do have the magnitude expected for an angle of attack close to $90^{\circ}$ during both the up and down-leg portion of the path.

Ion Concentration

For convenience of analysis the flight plane has been taken as the y z plane (Figure 11). The z axis is the radius of the earth through apogee. The angles which the total angular momentum vector makes with the x, y and z axes are $\beta_1$, $\beta_2$, and $\beta_3$ respectively. These angles remain constant for the portion of the flight path of interest here. The symmetry axis of the rocket precesses about $\bar{L}$ with a constant period provided the rocket may be considered a rigid body. The angle which the axis makes with $\bar{L}$ is designated $\gamma$.

With the retarding potential less than or equal to zero, the current to the ion trap is proportional to the total flux of ions to the forward face of the rocket. The current is given by the formulae

$$I = eA\, v \cos\theta \sum_i N_i D(v\cos\theta, \alpha_i)\, D(v\cos\theta, \alpha)$$

$$= 1/2 + 1/2 \operatorname{erf} \frac{v\cos\theta}{\alpha} + \frac{\alpha}{2\sqrt{\pi} v\cos\theta} \cdot \exp - \left(\frac{v\cos\theta}{\alpha}\right)^2$$

$$\alpha_i^2 = \frac{2kT}{M_i}$$

where e is the electronic charge; A, the effective ion trap entrance area; v, the rocket velocity; $\theta$, the angle of attack; $N_i$, the concentration of the ith ion; T, the common ion temperature; and M, the ion atomic weight. The cosine of the angle of attack was computed assuming that the rocket behaved as a rigid body with no applied torques. Since no attitude devices had been included in the payload, it was necessary to try different assumptions as to the values of $\gamma$, $\beta_1$, $\beta_2$, $\beta_3$, and the precession period.

A dynamical relationship exists between the ratio of precession period to spin period, ratio of moments of inertia, and the precession cone angle. This relation was of no assistance since the moments of inertia of combined payload and burned out rocket motor are not available, and the spin period is not known.

With failure of the light ion mass spectrometer to provide data, it was also necessary to make some assumption concerning the relative concentration of ions. $O_{16}^+$ ion are known to be the dominant ion in the lower portion of the rocket flight and $H^+$ ions are expected to dominate at apogee. $He^+$ ions may be present, but the extent is uncertain. In view of the uncertainties, a model ionosphere consisting of only two ionic species in diffusive equilibrium was assumed in deriving ion concentrations from the ion current data. Evidence from the Ariel I satellite (Bowen, et al. 1964B) indicates that the transition from $O_{16}^+$ ions to the lighter ion occurs at approximately 600 km

altitude at the local time and solar cycle phase appropriate to the flight time of the rocket flight. The variation of ion current amplitude with altitude also makes it clear that the transition altitude is close to 600 km. Consequently, the ratio of ion concentrations was assumed to be consistent with an isothermal ionosphere in diffusive equilibrium and to have the value one at 600 Km altitude. The ratio may be shown to be

$$\frac{N_1}{N_2} = \exp\left[(z-z_o)\,\frac{H_1 - H_2}{H_1 \cdot H_2}\right]$$

where

$$H_i = \frac{kT}{M_i g}$$

and

$$Z = \frac{Rh}{R + h}\,.$$

h is the altitude, R, the radius of the earth, and g, the acceleration of gravity (Hanson, 1962). The temperature was assumed to be 1000°K, a value which proved close to the measured ion temperature at apogee.

The period of precession of the rocket cannot be inferred unambiguously from the graph of ion current amplitude vs time (Figure 10) alone. The graph represents the time behavior of the ion current when sampled at a rate of once every 1.63 seconds. If the actual precession period were 1.87 sec, a 12.8 second period would be observed in the sampled data. The behavior of the time derivative of the ion current sampled at the above rate is also illustrated in Figure 10. The derivative has a maximum negative value when the amplitude is increasing and maximum positive value when the current amplitude is decreasing. This behavior can only be explained by assuming that the actual ion current was varying with a period, $\tau_m$, such

that the sample period, $\tau_s$, satisfies the relation

$$(n-1/2)\ \tau_m < \tau_s < n\,\tau_m \qquad n = 1, 2 \ldots$$

The apparent period of the sampled data $\tau_a$ is given by

$$\frac{1}{\tau_s} - \frac{1}{n\tau_m} = \frac{1}{\tau_a}$$

or

$$\tau_m = \frac{\tau_a \tau_s}{n(\tau_a - \tau_s)}$$

assuming n = 1, and using 12.8 sec and 1.63 sec for $\tau_a$ and $\tau_s$ yields a value of 1.87 for $\tau_m$. If we let A represent the amplitude of the ion current modulation and B the amplitude of the time derivative of the ion current, then the ratio of B to A must satisfy the relationship

$$\frac{B}{A} = \frac{2\pi}{\tau_m}$$

This ratio, estimated from Figure 10 to have the value, 3, yields a value of approximately 2 for $\tau_m$, a value close to that derived above for n = 1.

The total concentration profile illustrated in Figure 12 was computed assuming that the precession cone angle was zero and the axis of the rocket was in the plane of the trajectory and tangent to the flight path at about 550 km on the up leg of the trajectory. The atomic mass of the light ion was taken as 2 gram/mole. The electron concentration profile reduced from an ionogram taken at the time of the flight is also recorded. It is quite

evident that the rocket did not behave in the desired way - i.e., with a small angle of attack on the up leg. The low concentration computed for the up leg and the high concentration for the down leg reflect the fact that the current to the ion trap was an order of magnitude smaller than it should have been for a small angle of attack on the up leg and two orders of magnitude too large for the down leg. The scatter in concentration indicated by bars results from the periodic variation in ion current amplitude evident in Figure 10.

The fact that the ion current is approximately of the same amplitude on both up and down legs at corresponding heights near the F peak (Fig. 10) indicates that the angle of attack should be essentially the same for both ends of the rocket trajectory. A rocket motion satisfying this requirement is one in which the precession cone angle is small and $\bar{L}$ is at right angles to the flight plane. Figure 12 illustrates the total ion concentration computed with the assumption that the rocket axis was at right angles to the flight plane at all times. The concentration on both up and down legs is approximately the same and is consistent with the value deduced from an ionosonde.

The computed charge concentration at apogee is nearly independent of assumed rocket attitude since the rocket is moving at approximately one third the ion thermal velocity at that altitude. The concentration depends primarily on the assumed atomic mass of the ions. The lower concentration obtained by assuming an atomic mass of one is in better agreement with mean concentration values measured at midnight, at 1000 km, and at $53^{\circ}$ North

dip latitude by the Alouette satellite (private communication with K. L. Chan). The Explorer XXII satellite measured electron concentrations in the vicinity of Wallops Island at midnight and 1000 km altitude within the range of 0.5 to 1.5 x $10^4$ electrons/$cm^3$ (private communication with L. H. Brace). The ion concentration computed for either one or two grams/mole ionic mass fall within this range.

Several additional concentration profiles have been computed with different values of $\gamma$, $\beta_1$, $\beta_2$, and $\beta_3$ having the values $12^\circ$, $0^\circ$, $90^\circ$, and $90^\circ$ respectively and with an apparent precession period of 12.8 seconds. Figure 13 illustrates the partial and total concentration computed assuming the upper ionosphere to be composed of hydrogen ions only - no helium ions - and with $\gamma$, $\beta_1$, $\beta_2$ and $\beta_3$ having the above values.

Ion Temperature

The ion temperature has been computed by fitting the theoretical expression for the ion current to a hemispherical ion trap given by Knudsen and Sharp (1965) to the characteristic curves obtained near apogee. Although the theoretical expression was derived assuming the angle of attack zero, it is accurate when the ratio of vehicle velocity to ion thermal velocity is small. Put another way, angle of attack has no significance for a stationary vehicle. At apogee this ratio is 0.2 provided the ions are protons. With the use of the correct theoretical equation for angle of attack of $90^\circ$, it has been verified that a velocity ratio of 0.2 is small enough to neglect without significant error.

If the vehicle may be assumed at rest, i.e., the velocity ratio negligible, the temperature which is computed is independent of mass. All ions regardless of mass have the same energy distribution and it is the energy distribution that determines the temperature. Hence, the ion tem-

perature derived is independent of assumed mass.

Figure 14 illustrates the data points for one of the characteristic curves and the theoretical curve computed using the least-squares-adjusted parameters. Figure 15 illustrates the values of ion temperature and vehicle potential obtained in like manner for several consecutive characteristic curves at apogee. Some of the indicated variation is probably caused by changes in angle of attack which is not entirely negligible. The error bars are statistical uncertainties based on the scatter of the data points for each characteristic curve and do not represent absolute uncertainty. In what follows, the ion temperature will be taken as 1100°K and the vehicle potential as -0.50 volts.

An electron temperature may be estimated from the vehicle potential if certain assumptions are made. The electrons are assumed to have a Maxwellian velocity distribution with a temperature, $T_e$, the vehicle potential is assumed constant over the conducting surfaces of the vehicle, and the rectification of the radiated telemetry signal is assumed negligible. The uniform potential assumption requires that $\bar{v} \times \bar{B}$ fields are small and that the work function of the conducting surfaces is the same as that of gold. The majority of the conducting surface of the vehicle consisted of the gold plated instrument section and, if the instrument section were the more positive end of the vehicle, the effect on vehicle potential of the small conducting ring near the nozzle of the last stage engine could be neglected. The $\bar{v} \times \bar{B}$ field would be of the order of 0.05 volt/meter and, with an instrument section approximately a meter long, vehicle potential variations of the order of a few hundredths of volts are expected. A telemetry rectification potential of

-0.2 volts has been observed on small packages (Nagy and Faruqui, 1965).

Equating electron and ion fluxes, one obtains

$$\sqrt{\frac{kT_i}{2\pi m_i}} = e^{\frac{e\varphi}{kT_e}} \sqrt{\frac{kT_e}{2\pi m_e}}$$

and,

$$T_e \simeq 1500^{\circ}$$

where $m_i$ has been taken as 1 gm per mole.

Bowen et al. (1964A) report electron temperatures measured at 1000 kilometer during 1962. The value reported for midnight at 60°N geomagnetic latitude for magnetically quiet days is approximately 1350°K.

The electron temperatures measured by the Explorer XXII satellite for the local time, altitude, season, and year appropriate to the 8.03 rocket flight fall within the range, 1500° - 2000°K (L. H. Brace, private communication).

The ratio of electron to ion temperature, $T_e/T_i$ is expected to reach unity at a sufficiently high altitude. (Hanson, 1963) and recent calculations by Brace et al. (1965) suggest that at 1000 km the ratio would be essentially one.

The ratio obtained from the ion and electron temperature reported herein is

$$\frac{1500}{1100} \simeq 1.4$$

This value is primarily uncertain because of the uncertainty in the electron temperature.

Conclusions

To obtain consistent ion concentrations in the F region for both up and down legs of the rocket trajectory, it is necessary to assume that the rocket axis made an angle close to $90^{\circ}$ with the plane of trajectory throughout the flight. With this assumption, the concentration measured at the F peak on the up leg is equal to that observed with an ionosonde within the uncertainty to which the instrument transmission factor is known. The ion concentration computed at apogee depends on the assumed ionic atomic mass. With $H^{+}$ as the dominant constituent a concentration of $8 \times 10^{3}$ is obtained - a value consistent with other observations. The ion temperature at apogee (1013 km) is $1100^{\circ}K$ with an estimated uncertainty of 10 percent. This temperature value is not sensitive to the assumed ionic mass. An electron temperature of $1500^{\circ}K$ may be computed from the observed vehicle potential upon making several assumptions. The uncertainty is estimated to be 40%.

Mass Spectrometer Analysis and Interpretation

A discussion of the operation of the Ion Mass spectrometer is presented earlier in this report. For the detailed theory of the operation of the quadrupole Mass spectrometer the reader is referred to the literature (Paul, et al, 1958; Brubaker, 1961; Flowerday, 1964).

The mass spectrometer was mounted on the nose plate of the rocket with its axis parallel to, but displaced from, the spin axis. The entrance apperture of the spectrometer had a diameter of 0.2 inches. An accelerating potential of -20 volts was applied to a screen located inside the grounded

instrument entrance screen and preceeding the quadrupole analyzer such that ions entering the spectrometer would have velocities essentially parallel to the spectrometer axis. The RF voltage applied to the rods was "slaved" to the applied DC voltage so that the ratio of the two was kept constant during a sweep. The telemetry output was calibrated with a mixture of gases and was indeed linear as a function of mass number. The period of the sweep, up and down, was 1.95 sec. On the upsweep, the DC voltage was monitored on the telemetry output and on the downsweep the RF voltage was monitored on the telemetry output.

The overall transmission efficiency of the ion mass spectrometer was measured in the laboratory, for zero angle of attack, as a function of mass number. Typically, for 3 volt mass 16 ions the transmission efficiency was found to be approximately 9%.

The rocket flight orientation has been discussed in the section on the ion trap. This topic will further be considered and its effect on the ion mass spectrometer output in a later discussion.

Telemetry Output

The form of the data is presented in Figure 16 which is a section of the actual telemetry record. The line designated "sweep" represents the value of the voltage applied to the electrodes of the quadrupole spectrometer as a function of time. The upward sweep is a monitor of the DC voltage whereas the downward sweep indicates the RF voltage which is at all times "slaved" to the DC voltage to obtain a constant value of the ratio of DC to RF voltage.

The line segment marked "range" indicates the range of the electrometer output of the spectrometer. On the extreme right-hand side of the figure one notes that a range change has taken place commensurate with the detection of a large mass peak. The output of the electrometer of the spectrometer is indicated as the signal. Several mass peaks have been identified and are labeled accordingly. The telemetry record gives every indication that the ion mass spectrometer was functioning properly throughout the course of the flight.

Vehicle Orientation

The ion mass spectrometer experiment was designed to fly with a reasonably small angle of attack on the ascent of the rocket. As has been pointed out previously in the section discussing the ion trap measurements, it does not seem possible that the vehicle acquired its intended orientation. It appears considerably more likely that the orientation of the vehicle was such that the spin axis was at right angles to the flight path and was precessing about its spin axis (see Figure 11 and the accompanying discussion). Further evidence for this presumed orientation is presented from the mass spectrometer data. In Figures 17 and 18 are plotted the ion currents corresponding to the observed peaks, as a function of the vehicle flight time. It is observed that periodic structure to the data exists and that for each peak the period is approximately 35 sec. This varying amplitude could have been caused by the proposed precession of the vehicle.

If the vehicle is precessing with a period $\tau_m$ and the data is periodically sampled with a sampling period $\tau_s$ then it can easily be shown that the apparent

period of the sampled data, $\tau_a$, is given by

$$\tau_a = \frac{n\,\tau_m\,\tau_s}{n\,\tau_m - \tau_s} \tag{7}$$

where n is an integer and allows for the possibility of sampling a harmonic of $\tau_m$. Using this expression with $\tau_a$ = 35 sec, $\tau_s$ = 1.95 sec and n = 1 we find that $\tau_m$ is 2.06 sec. This value for $\tau_m$ is in reasonable agreement with that found from the ion trap measurements. In this calculation the value for $\tau_s$ is taken for a given peak only on the "upsweep" of the data. For the same peak on the downsweep the sampling period, $\tau_s'$ would have the same value, however, there would be a phase shift in the apparent period $\tau_a$ from the upsweep apparent period $\tau_a$.

The apparent phase shift is given by

$$\Phi = \frac{(\Delta\tau_s + \tau_m - \tau_s)}{\tau_m} - \frac{(\tau_s + \Delta\tau_s)}{\tau_a} \tag{8}$$

where $\Delta\tau_s$ is the time delay from a given mass peak on the upsweep data to the same mass peak on the downsweep data. In the case of mass peak 18 $\Delta\tau_s$ is 1.65 sec., this gives a value for $\Phi$ of 0.83 when $\tau_s$ = 1.95 sec. and $\tau_m$ = 2.06 sec. Thus an apparent shift in the positions of maximum amplitude of the time varying signal of the downsweep data, compared with the upsweep data, should be 29.1 sec. The data for mass peak 18 was analyzed over a portion of the range for both upsweep and downsweep and the apparent shift of the amplitude peak was found to be approximately 30 sec.

These considerations along with those presented in the section on the ion trap strongly indicate that the only possible orientation of the vehicle is that presumed above.

The precession cone angle, $\gamma$, can be determined from the variation in the amplitude of the ion current. The ion current incident upon the entrance aperture, having zero retarding potential relative to the plasma, is given by

$$I_i = K_i N_{o_i} e V \cos\theta A \left\{ 1/2 + 1/2 \operatorname{erf} \frac{(V \cos\theta)}{\alpha_i} + \frac{\alpha_i}{2\sqrt{\pi}\, V \cos\theta} \exp\left[-\left[\frac{V \cos\theta}{\alpha_i}\right]^2\right]\right\} \quad (9)$$

where $N_o$ is the ambient ion density of the ith kind, e is the electronic charge, A is the area of the entrance apperture, V is the total vehicle velocity, $\theta$ is the angle the total velocity vector makes with the normal to the plane of the entrance apperture, $\alpha_i$ is the most probable velocity of the ambient ith ions, and $K_i$ is the spectrometer transmission factor for ions of the ith kind.

For $\theta = \theta$ min the ion current $I_i$ is a maximum, whereas for $\theta = \theta$ max the ion current $I_i$ is a minimum, and since $\theta$ max $= \pi - \theta$ min and $\theta$ min $= \left(\frac{\pi}{2} - \gamma\right)$ then

$$\frac{I_i \max + I_i \min}{I_i \max - I_i \min} = \operatorname{erf}\left(\frac{V \sin\gamma}{\alpha_i}\right) + \frac{\alpha}{\sqrt{\pi}\, V \sin\gamma} \exp\left[-\frac{(V^2 \sin^2\gamma)}{\alpha_i^2}\right]$$

Thus by measuring the relative magnitudes of the peaks and the valleys the precession angle $\gamma$ can be determined from a knowledge of the total vehicle velocity.

Upon considering the mass 16 peak on the descent portion of the flight the precession angle $\gamma$ was determined to be approximately $20^{\circ}$.

Results

Four distinct mass peaks were observed during the course of the vehicle flight. On the telemetry record, Figure 16, each of these is observed and labeled as mass peak 16, 18, 30 and 46 according to the pre-flight calibration of the ion mass spectrometer. It is observed in Figures 17 and 18 that the ion currents of the spectrometer associated with mass peaks 18, 30 and 46 are relatively large at the beginning of the flight but decrease throughout the flight except for a small increase near the very end of the flight. On the other hand, the spectrometer current associated with mass peak 16 is observed to be somewhat smaller than the other currents at the beginning of the flight and decreases in amplitude to a broad minimum at the top of the flight path which occurs at about 600 sec. On the descent of the vehicle the spectrometer current of peak 16 begins to increase and rises to a distinct maximum value, with value greater than any other current, at approximately 1000 sec., which corresponds to an altitude of approximately 370 km.

The data on the downward flight of the vehicle is consistent with present understanding of the structure of the ionosphere with $O_{16}^{+}$ being the dominant ion (Hanson, 1961). The fact that each of the other observed peaks generally decreases with time leads one to believe that these are contaminants associated with outgassing of the instruments or perhaps associated with a smoldering rocket after burn out. These contaminants may then undergo charge exchange and rearrangement collisions with the primary $O_{16}^{+}$ ions and then be detected

by the ion mass spectrometer. This could possibly account for the low value of the $O_{16}^+$ current observed on ascent of the vehicle through the F region as compared with the value observed on descent. On the ascent when the concentration of contaminants is greatest the $O_{16}^+$ ion near the instrument may be substantially depleted due to charge exchange with these contaminants, whereas on the return path through the F region the contaminant concentration is substantially reduced and hence the $O_{16}^+$ concentration is not depleted. Further evidence in support of this conclusion is that the sum of all currents on ascent is approximately the same as the sum of all current on descent.

The expression relating the ion concentration to ion current is given by Equation 9. The concentration of $O_{16}^+$ is determined as a function of altitude for only the downward portion of the flight and the results are presented in Figure 19.

Figure 19 is obtained by calculating ion concentrations at only the peaks values in the spectrometer current curves for $O_{16}^+$ with the assumption that the vehicle is in its most forward looking position, i.e. $\theta = \theta$ min, and $\gamma = 20^o$. The maximum value of the $O_{16}^+$ concentration is found to occur at an altitude of approximately 370 kilometers. Due to the nature of the vehicle motion and the problem of periodic samplings previously discussed, it is very possible that the peak of the F region was not detected. The ground based ionosonde measurements indicate the peak of the F region to be between 320-350 kilometers, and a maximum concentration of $8.8 \times 10^4$ ions/cm$^3$. This value is nearly a factor of 5 greater than the $O_{16}^+$ concentration as measured by the ion mass spectrometer. The smaller concentrations of $O_{16}^+$,

at the higher altitudes, are difficult to determine in that the ion currents are down in the noise and are thus hard to distinguish from the background. This gives rise to the scatter in the data at the higher altitudes.

The discrepancy between the ionosonde measurements and the ion mass spectrometer measurements may in part be explained by the possibility that the ion mass spectrometer did not pick up the F peak as discussed above. This argument cannot, however, account for the entire discrepancy. Laboratory experiments indicate that for a directed beam of ions the transmission factor of the spectrometer is dependent upon the angle of attack. Since the experiment was designed for $0^{\circ}$ angle of attack the effect on the transmission factor for large angles was not pursued and is not accurately known.

Conclusions

The ion mass spectrometer that was flown on the Javelin 8.03 vehicle did appear to be functioning properly. Ion mass peaks were detected and ion concentrations were measured. The vehicle did not assume the planned orientation which complicated the interpretation of the data. Ion mass peaks of mass number 16, 18, 30 and 46 were detected and mass numbers 18, 30 and 46 are presumed to be contaminants which charge exchange with the $O_{16}^{+}$ ions. The concentration of $O_{16}^{+}$ was measured as a function of altitude. The transmission factor of the ion mass spectrometer for large angles of attack is not adequately known, hence there exists a discrepancy between the absolute magnitude of the $O_{16}^{+}$ concentration at the F peak and ground based ionosonde measurements. For future use of the ion mass spectrometer on rocket flights, it will be necessary that the instrument be thoroughly

outgassed before operation and isolated from possible rocket engine contamination to suppress the detection of contaminants.

## GENERAL CONCLUSIONS

Although it was disappointing that all of the objectives of this program could not be met due to the failure of the Light Ion Mass Spectrometer in the Javelin 8.03 flight, nevertheless much useful scientific information has resulted from the studies of the structure of the ionosphere conducted under this contract. Probably the most startling result was the observation of temperature stratification in the E-region of the ionosphere observed on the Nike-Apache 14.110 flight. Further investigation into this phenomenon seems warranted to aid in the understanding of the physical processes which can cause such a stratification.

It is clear now that one cannot depend upon sounding rockets to behave as predicted and if rocket orientation is important then devices to determine the rocket orientation should be included in the rocket payload. The analysis of the Javelin 8.03 data was made very difficult because of the rocket behavior and also because the rocket angle of attack was not known.

Even with those difficulties, useful information has been obtained from the Javelin data. A total ion concentration profile was obtained over the altitude range of the rocket and ion temperature readings were computed near the peak of the rocket trajectory where the ion velocity exceeded the rocket velocity and vehicle orientation was not important.

A somewhat surprising result from the Javelin mass spectrometer was the extensive presence of ion contaminants caused, presumably, from rocket

outgassing and charge exchange reactions. This outgassing problem suggests the necessity of using some scheme for isolating the mass spectrometer from these outgassing products. Even with this problem and the unusual rocket motion it was possible tc obtain a well-defined profile for $O_{16}^{+}$ ions over the altitude range of the rocket. The presence of any ambient heavy ions was masked by the outgassing of the vehicle.

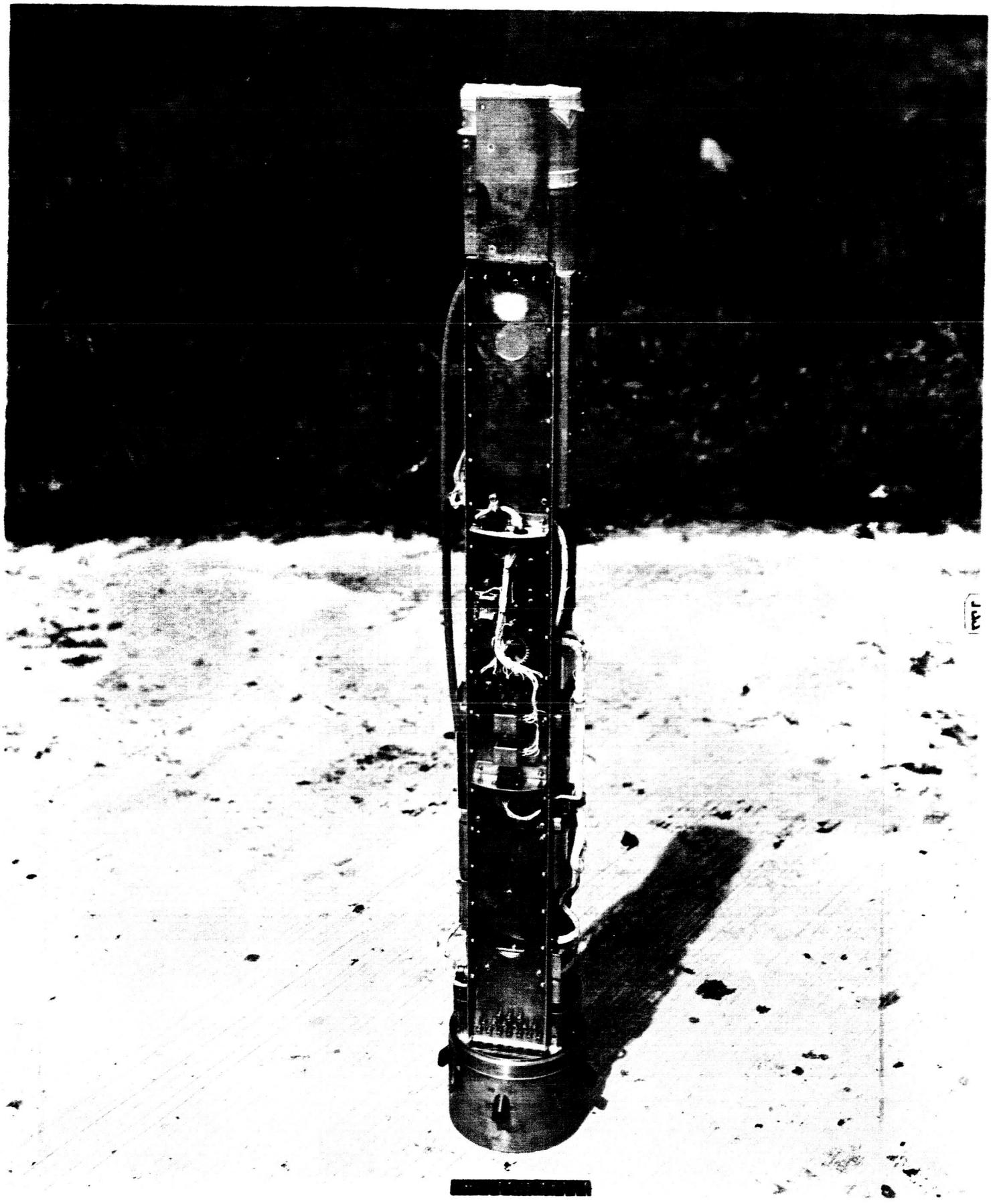

Figure 1

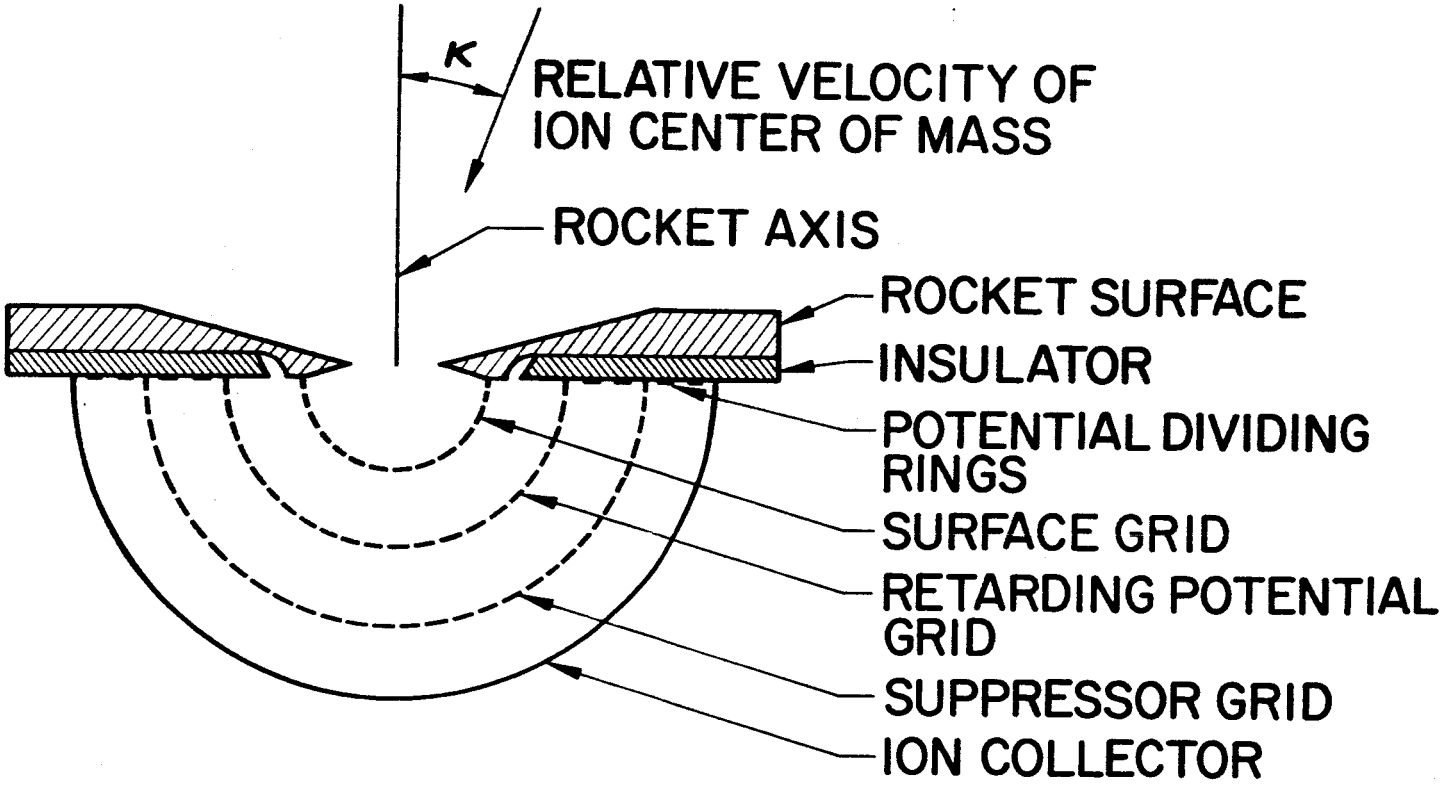
K
RELATIVE VELOCITY OF
ION CENTER OF MASS
ROCKET AXIS
ROCKET SURFACE
INSULATOR
POTENTIAL DIVIDING
RINGS
SURFACE GRID
RETARDING POTENTIAL
GRID
SUPPRESSOR GRID
ION COLLECTOR

Figure 2

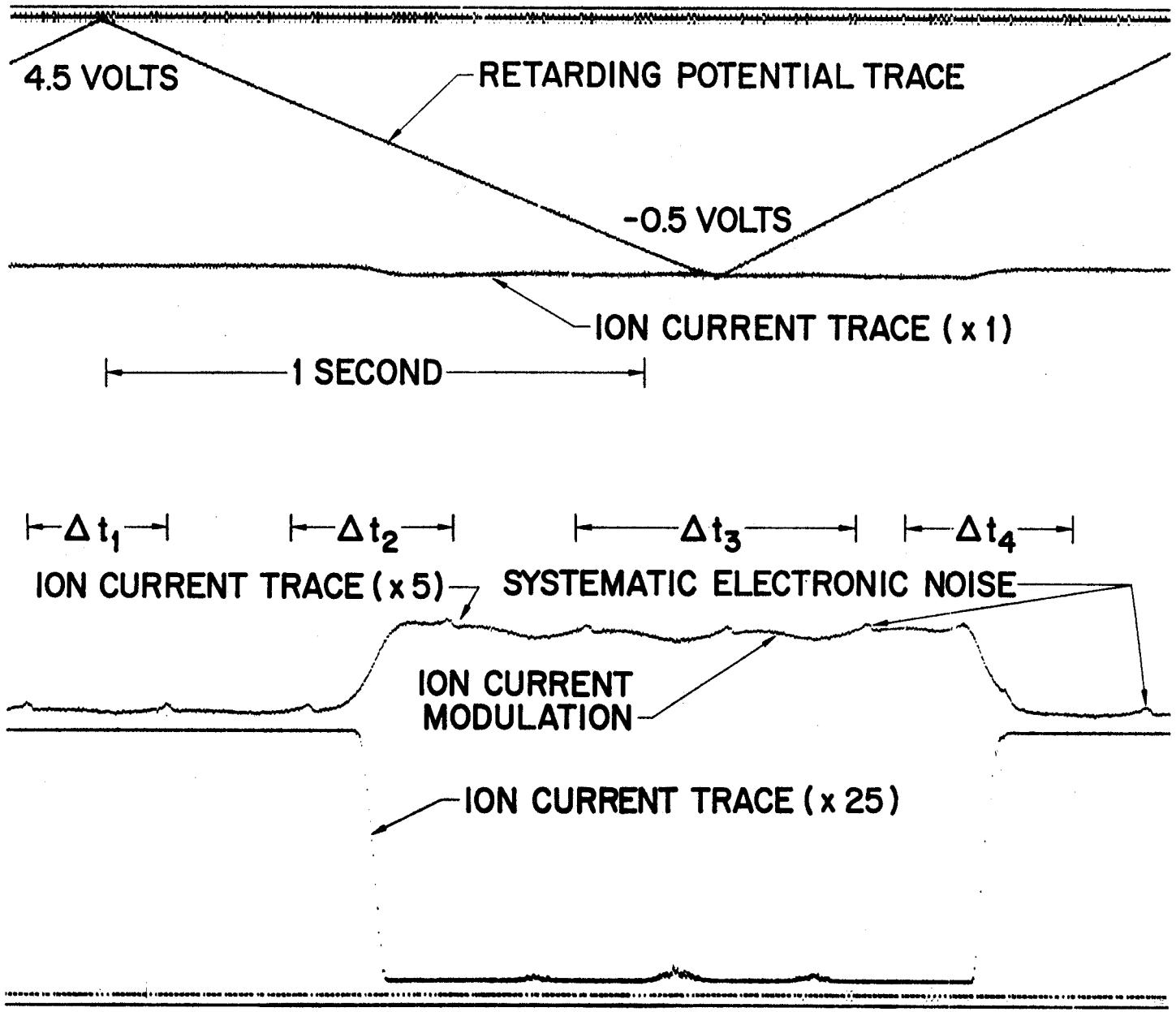
4.5 VOLTS
RETARDING POTENTIAL TRACE
-0.5 VOLTS
ION CURRENT TRACE (x 1)
1 SECOND
Δt1
Δt2
Δt3
Δt4
ION CURRENT TRACE (x 5)
SYSTEMATIC ELECTRONIC NOISE
ION CURRENT MODULATION
ION CURRENT TRACE (x 25)

Figure 3.

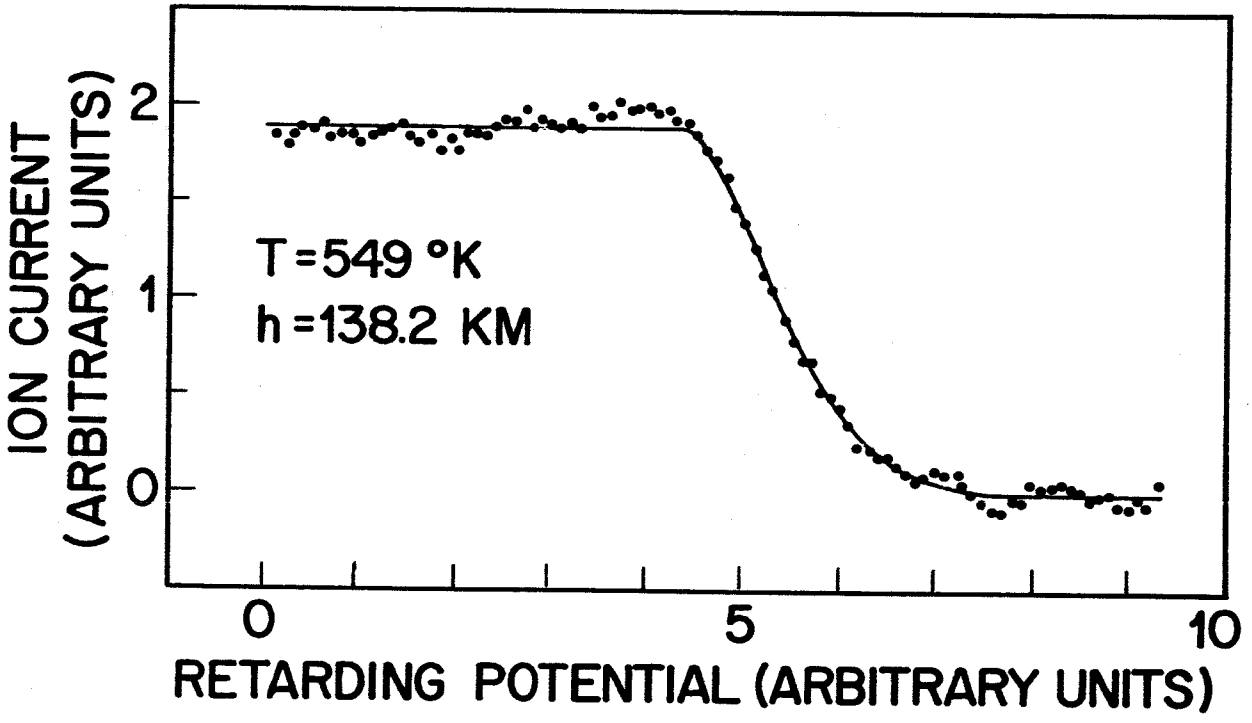
ION CURRENT
(ARBITRARY UNITS)
2
1
0
T=549 °K
h=138.2 KM
0
5
10
RETARDING POTENTIAL (ARBITRARY UNITS)

Figure 4

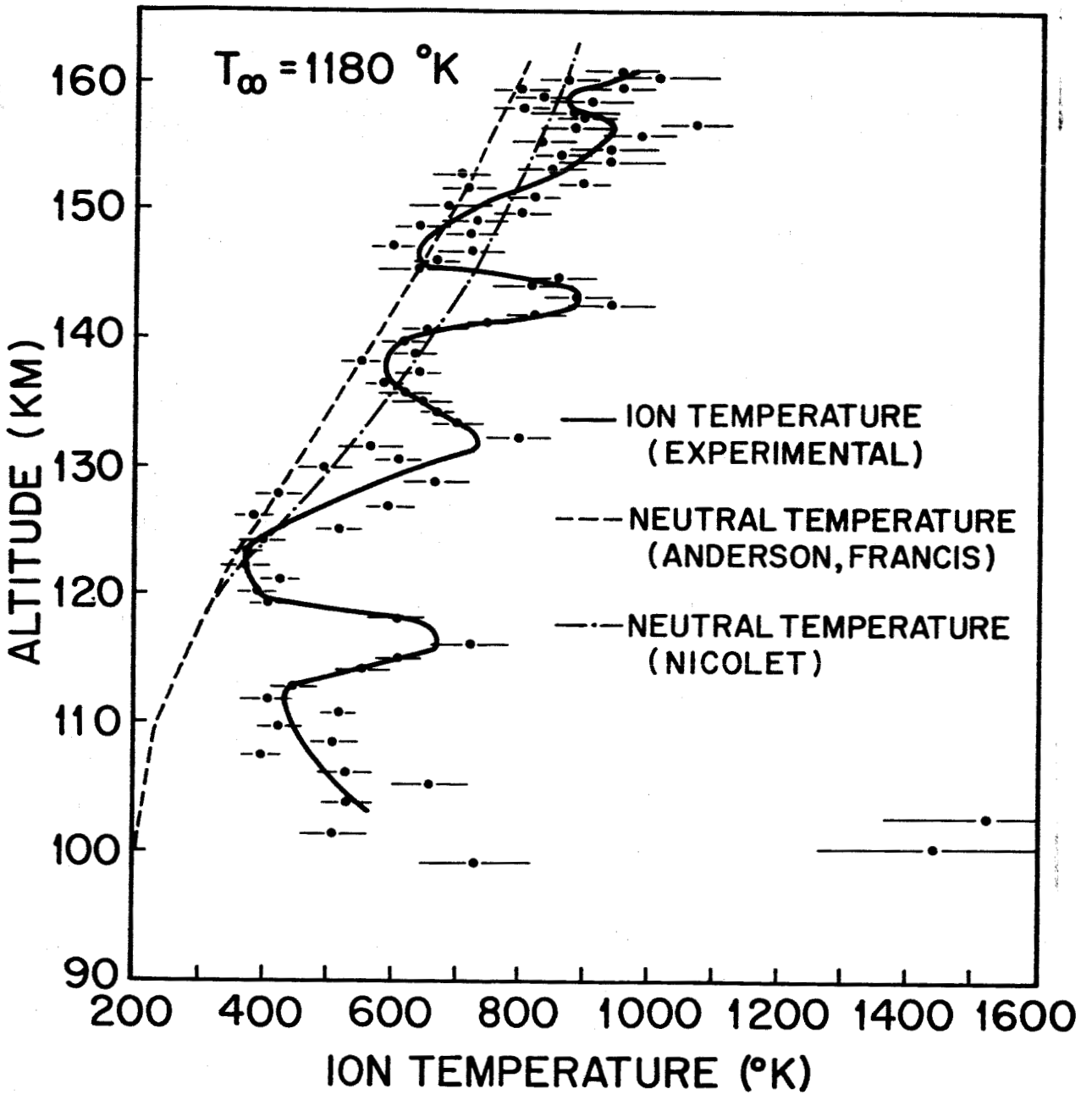
$T_\infty$ = 1180 °K
160
150
140
130
120
110
100
90
ALTITUDE (KM)
ION TEMPERATURE (EXPERIMENTAL)
NEUTRAL TEMPERATURE (ANDERSON, FRANCIS)
NEUTRAL TEMPERATURE (NICOLET)
200
400
600
800
1000
1200
1400
1600
ION TEMPERATURE (°K)

Figure 5

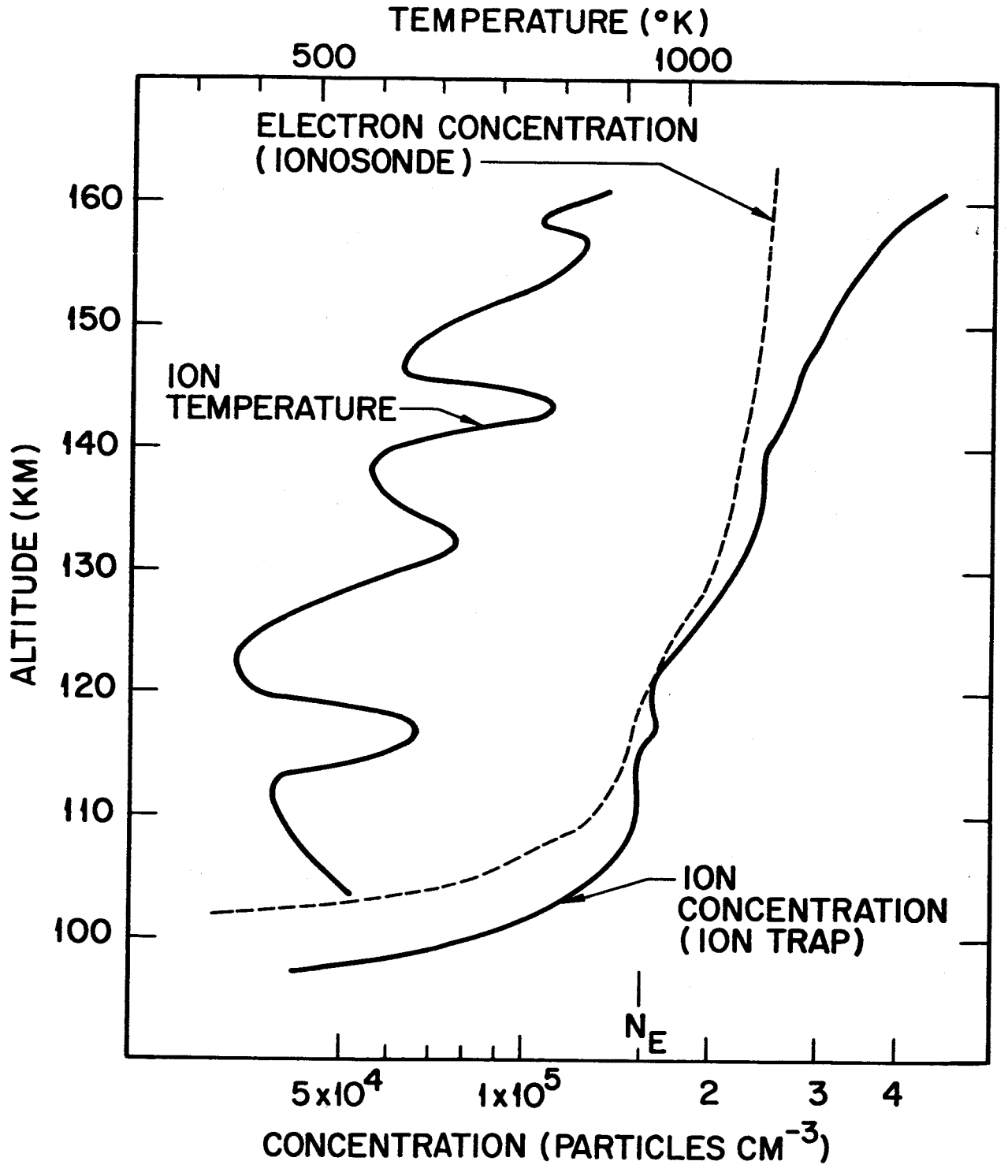
TEMPERATURE (°K)
500
1000
ELECTRON CONCENTRATION
(IONOSONDE)
ION
TEMPERATURE
ALTITUDE (KM)
160
150
140
130
120
110
100
ION
CONCENTRATION
(ION TRAP)
$N_E$
$5 \times 10^4$
$1 \times 10^5$
2
3
4
CONCENTRATION (PARTICLES $CM^{-3}$)

Figure 6

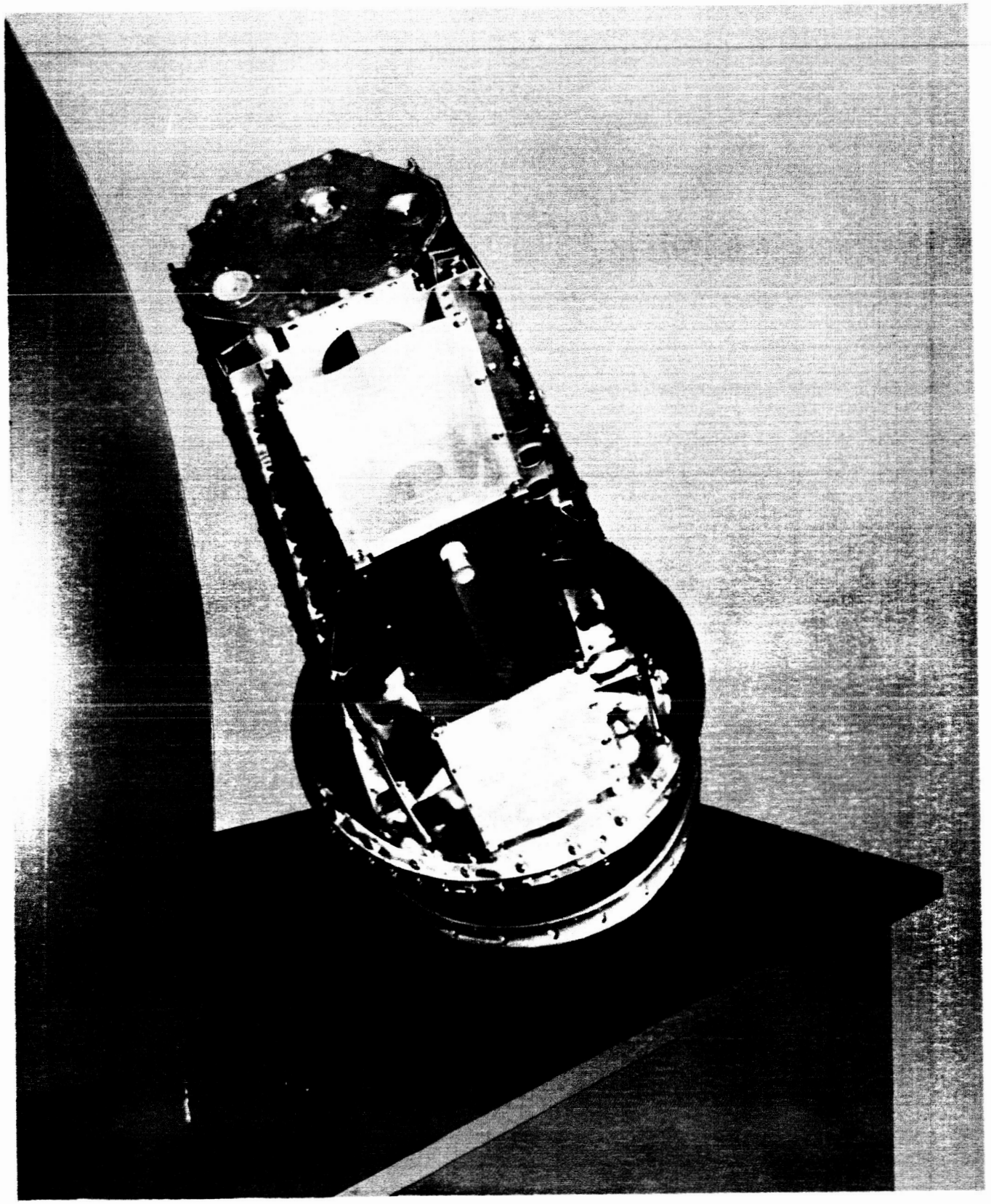

Figure 7

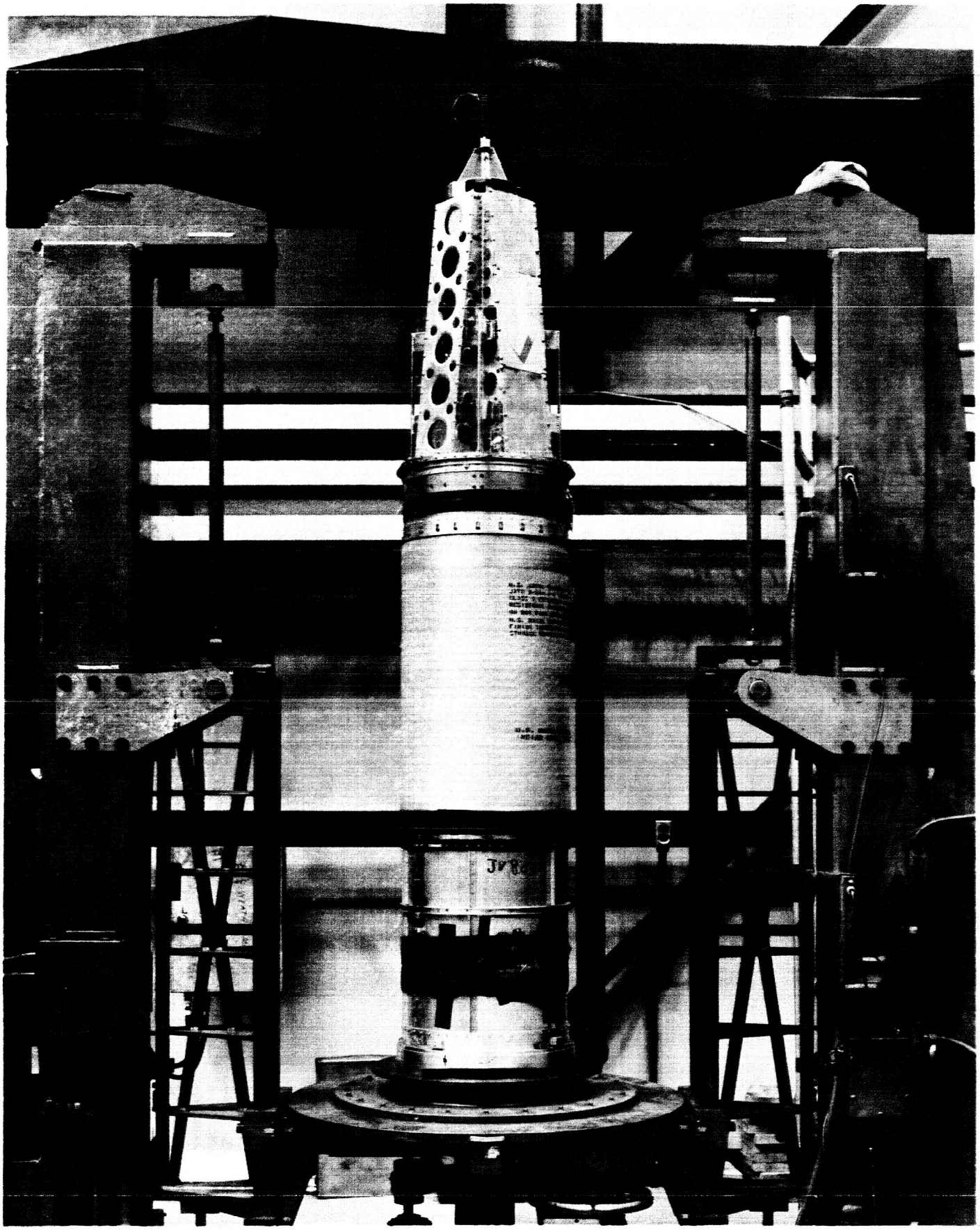

Figure 8

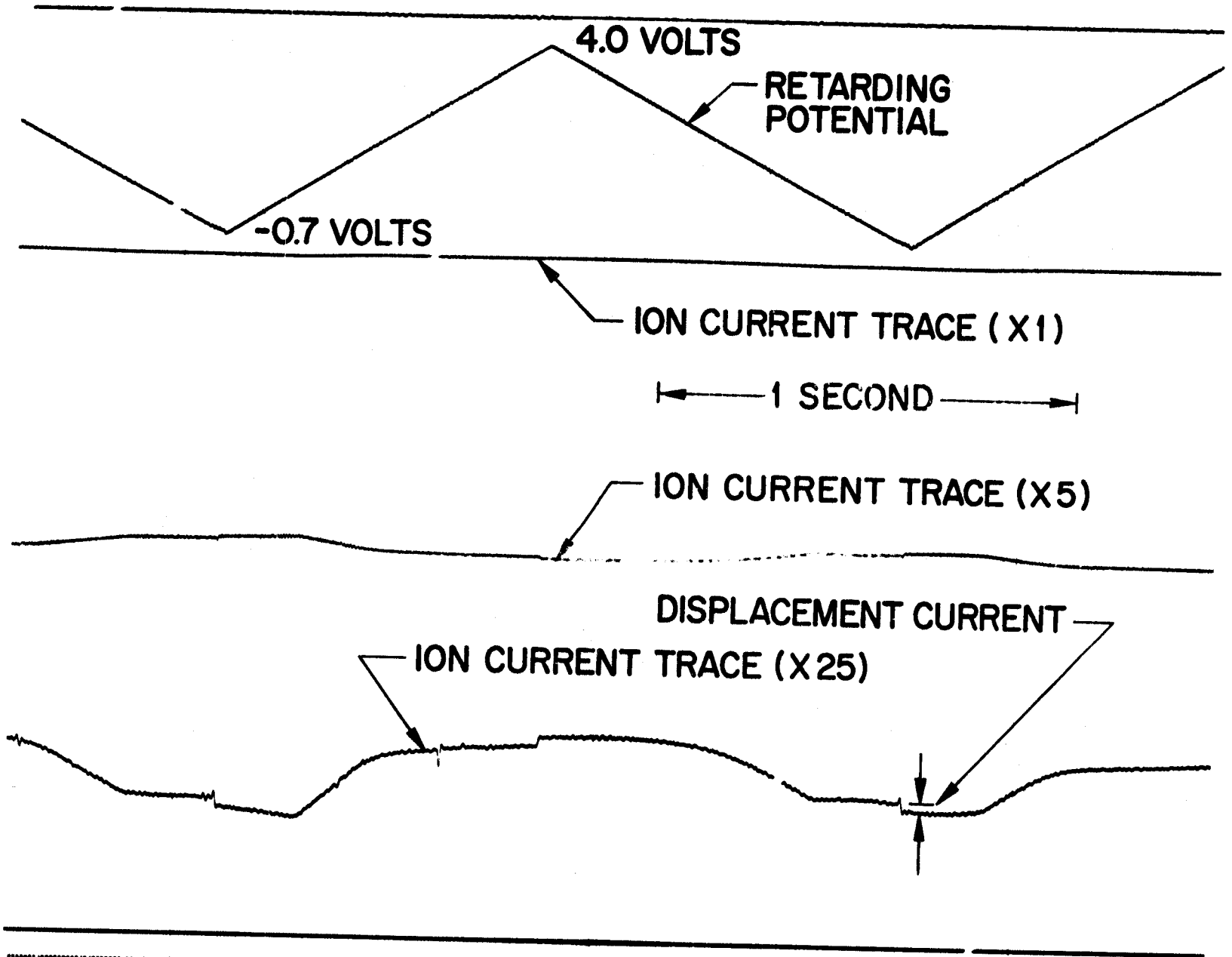
4.0 VOLTS
RETARDING POTENTIAL
-0.7 VOLTS
ION CURRENT TRACE (X1)
1 SECOND
ION CURRENT TRACE (X5)
DISPLACEMENT CURRENT
ION CURRENT TRACE (X25)

Figure 9

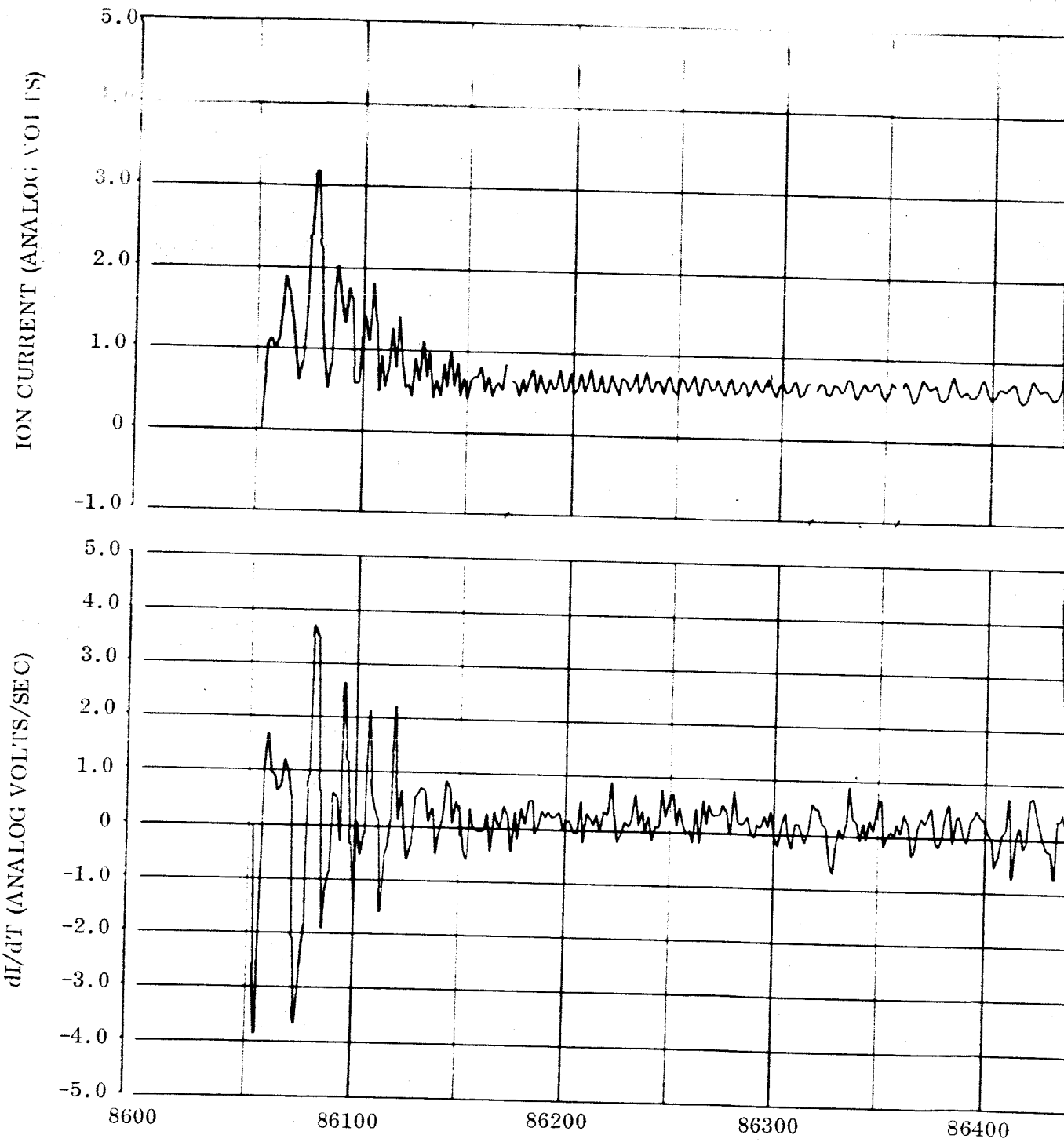
ION CURRENT (ANALOG VOLTS)
5.0
3.0
2.0
1.0
0
-1.0
dI/dT (ANALOG VOLTS/SEC)
5.0
4.0
3.0
2.0
1.0
0
-1.0
-2.0
-3.0
-4.0
-5.0
8600
86100
86200
86300
86400

2

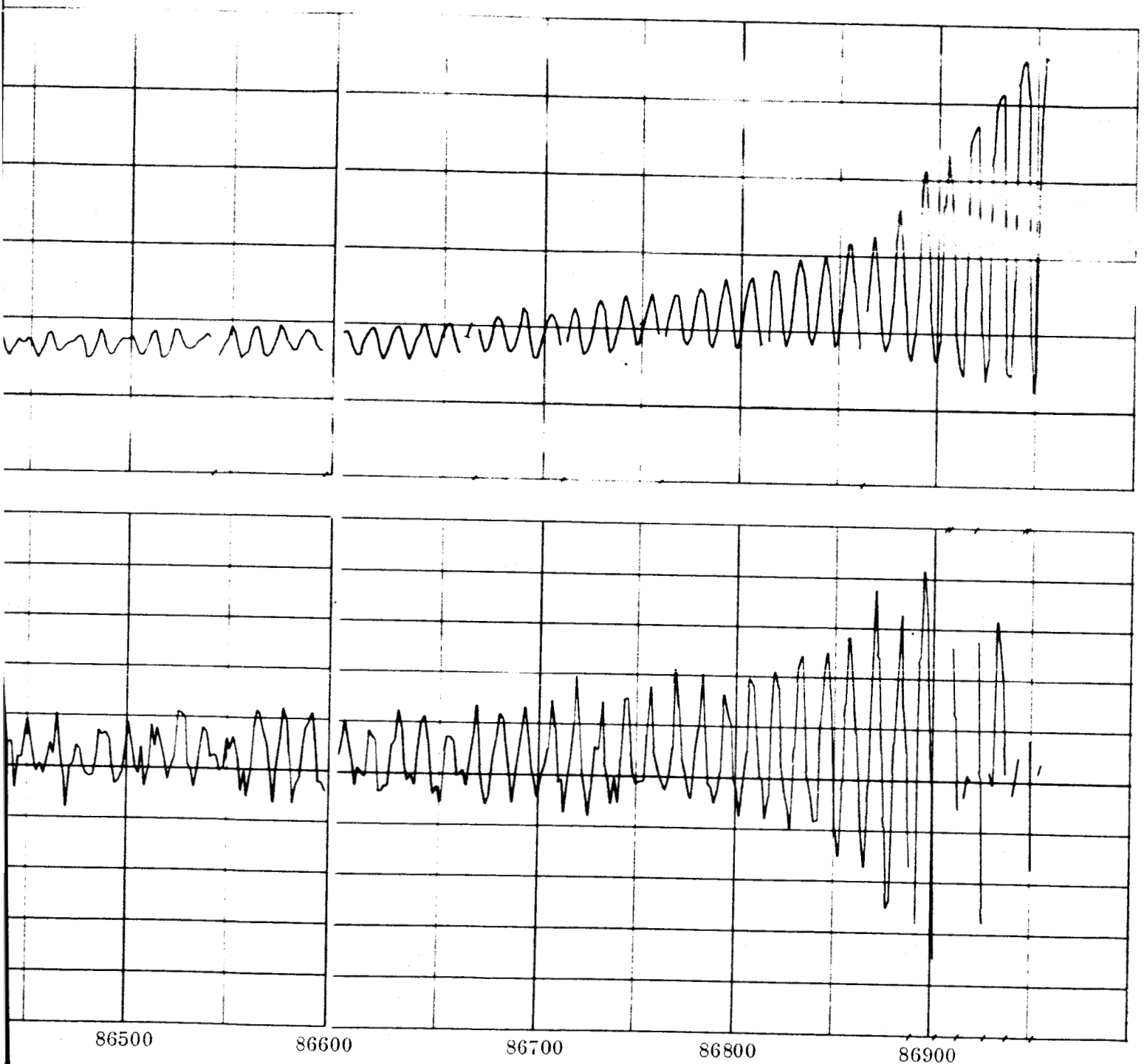


Figure 10

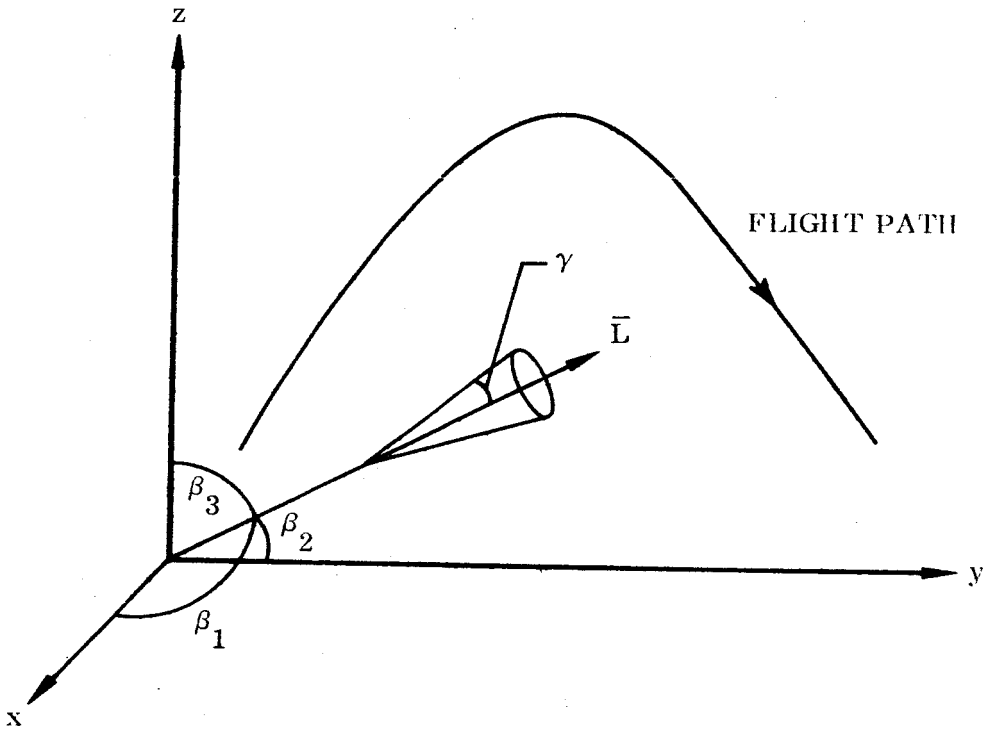


Figure 11

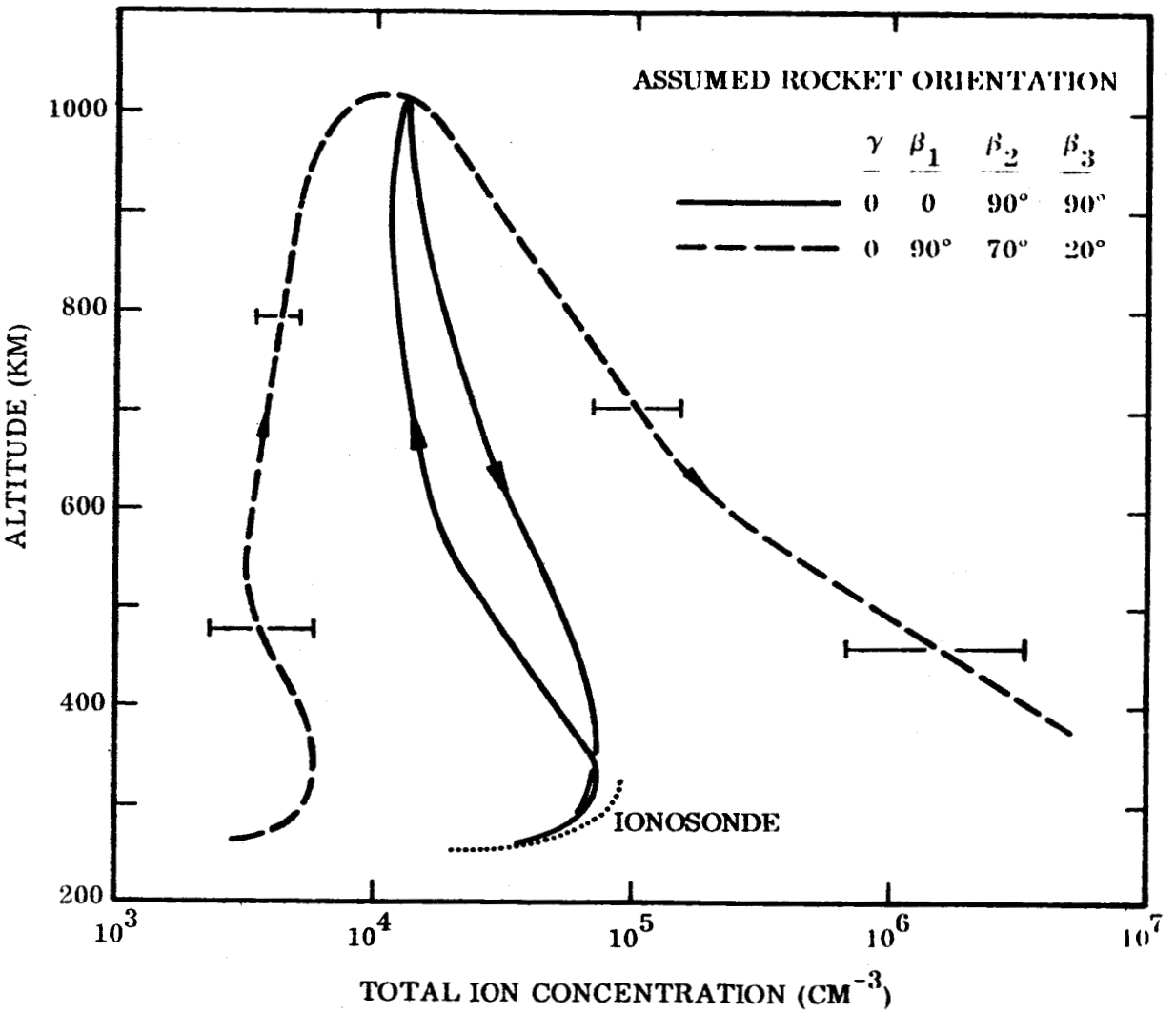
ASSUMED ROCKET ORIENTATION
γ β1 β2 β3
0 0 90° 90°
0 90° 70° 20°
IONOSONDE
ALTITUDE (KM)
1000
800
600
400
200
10^3
10^4
10^5
10^6
10^7
TOTAL ION CONCENTRATION (CM^-3)

Figure 12

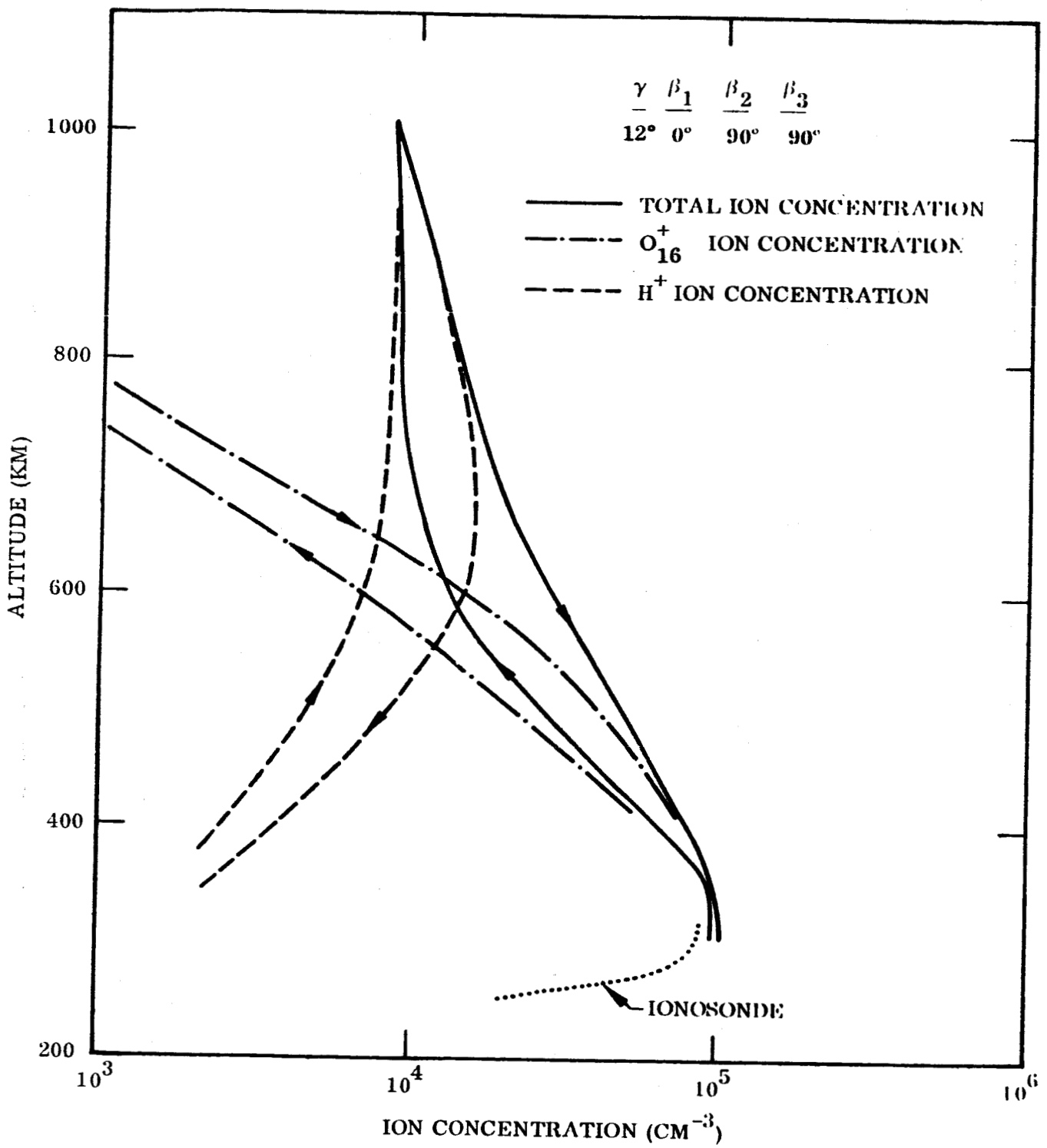
γ β1 β2 β3
12° 0° 90° 90°
TOTAL ION CONCENTRATION
O+16 ION CONCENTRATION
H+ ION CONCENTRATION
IONOSONDE
1000
800
600
400
200
ALTITUDE (KM)
10^3
10^4
10^5
10^6
ION CONCENTRATION (CM^-3)

Figure 13

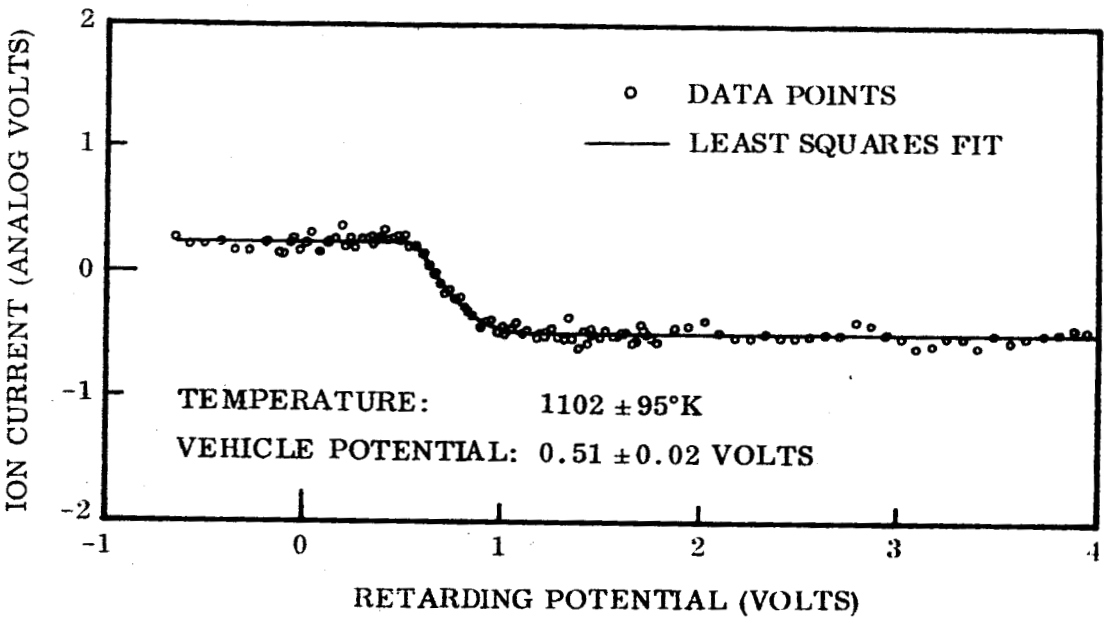
ION CURRENT (ANALOG VOLTS)
2
1
0
-1
-2
-1
0
1
2
3
4
RETARDING POTENTIAL (VOLTS)
DATA POINTS
LEAST SQUARES FIT
TEMPERATURE: 1102 ±95°K
VEHICLE POTENTIAL: 0.51 ±0.02 VOLTS

Figure 14

ALTITUDE: 1013 KM
LOCAL TIME: 2300 HRS
DATE: Oct. 8, 1964
DIP LATITUDE: 53°N

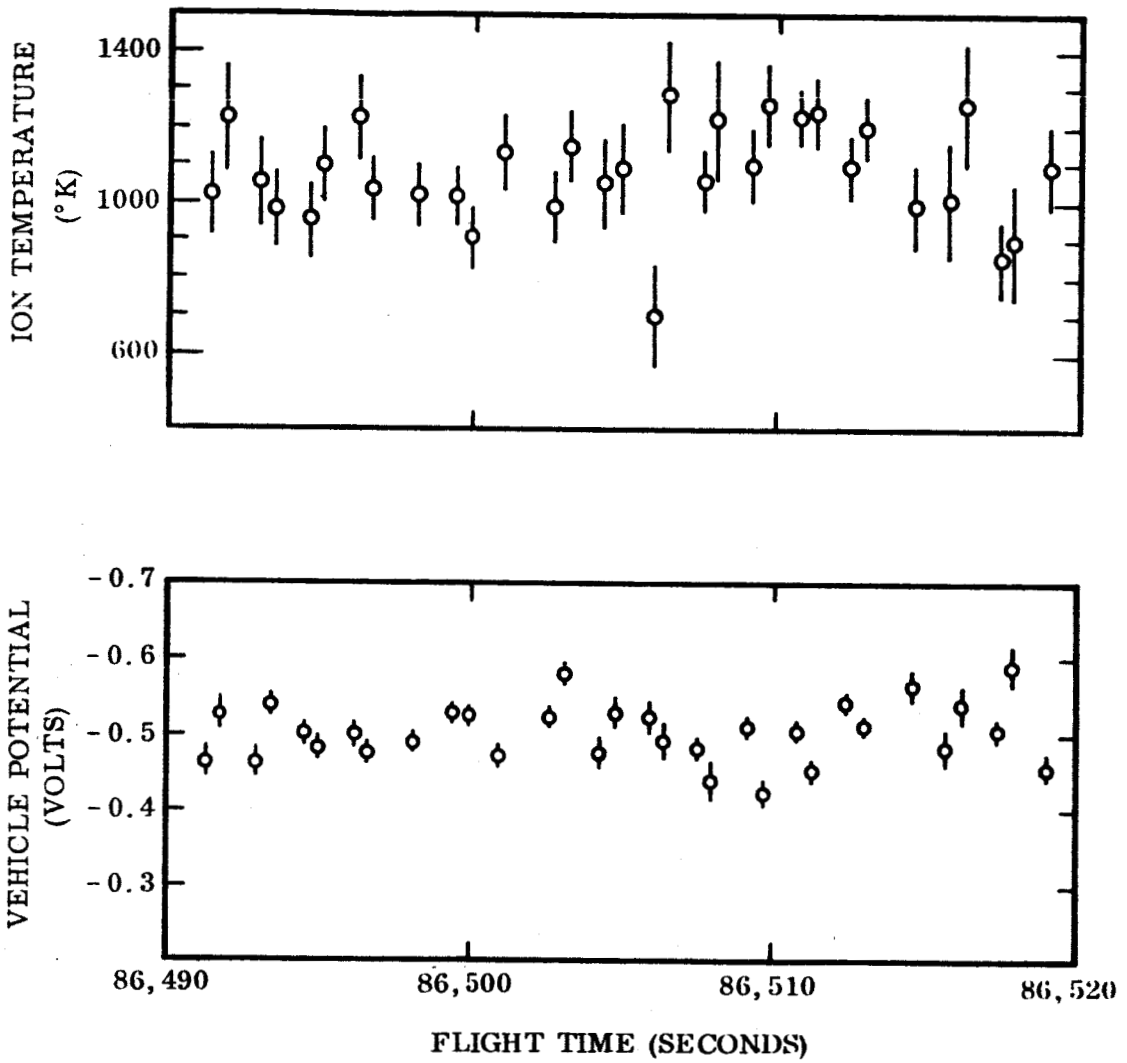


Figure 15

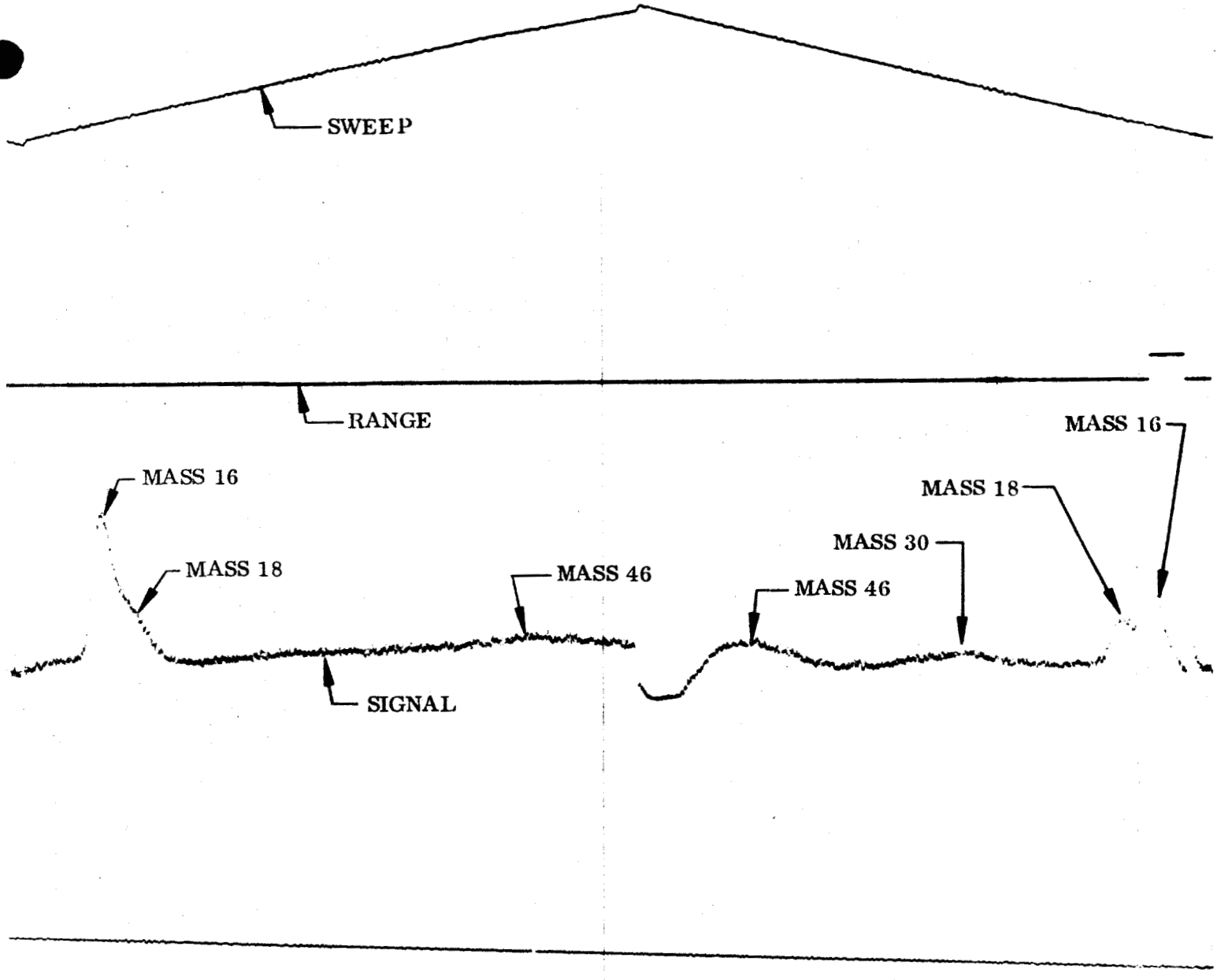
SWEEP
RANGE
MASS 16
MASS 18
MASS 46
SIGNAL
MASS 16
MASS 18
MASS 30
MASS 46

Figure 16

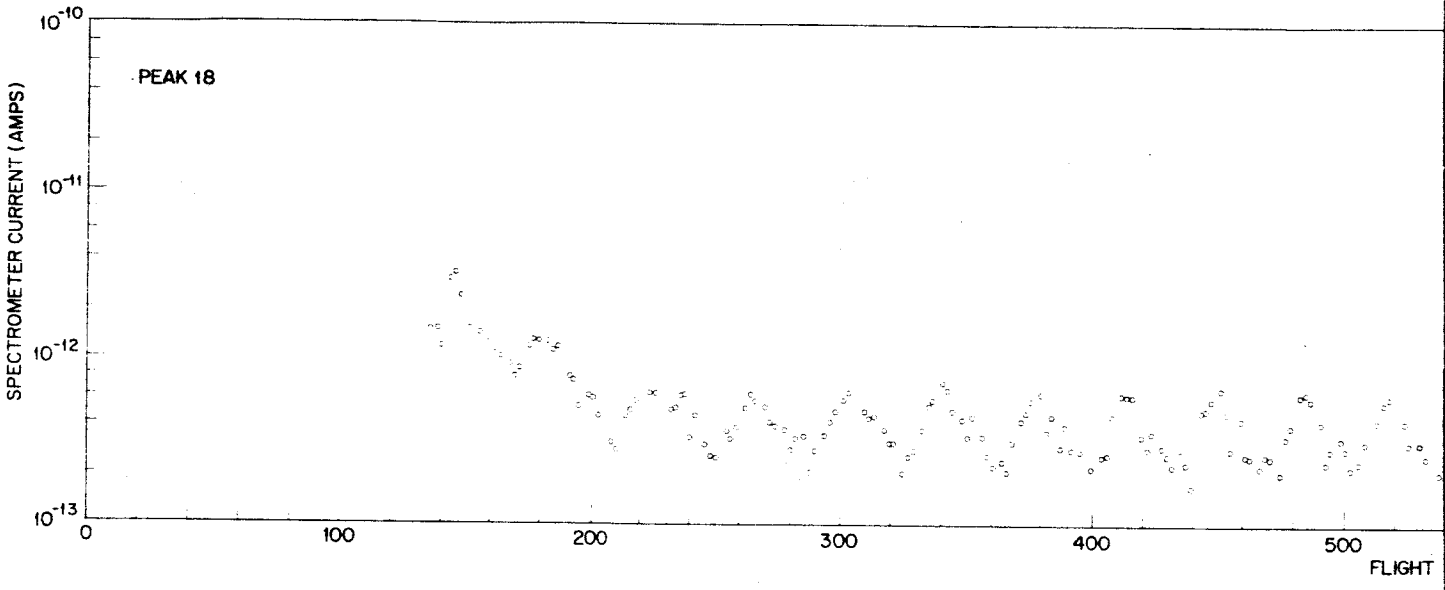
PEAK 18
SPECTROMETER CURRENT (AMPS)
$10^{-10}$
$10^{-11}$
$10^{-12}$
$10^{-13}$
0
100
200
300
400
500
FLIGHT

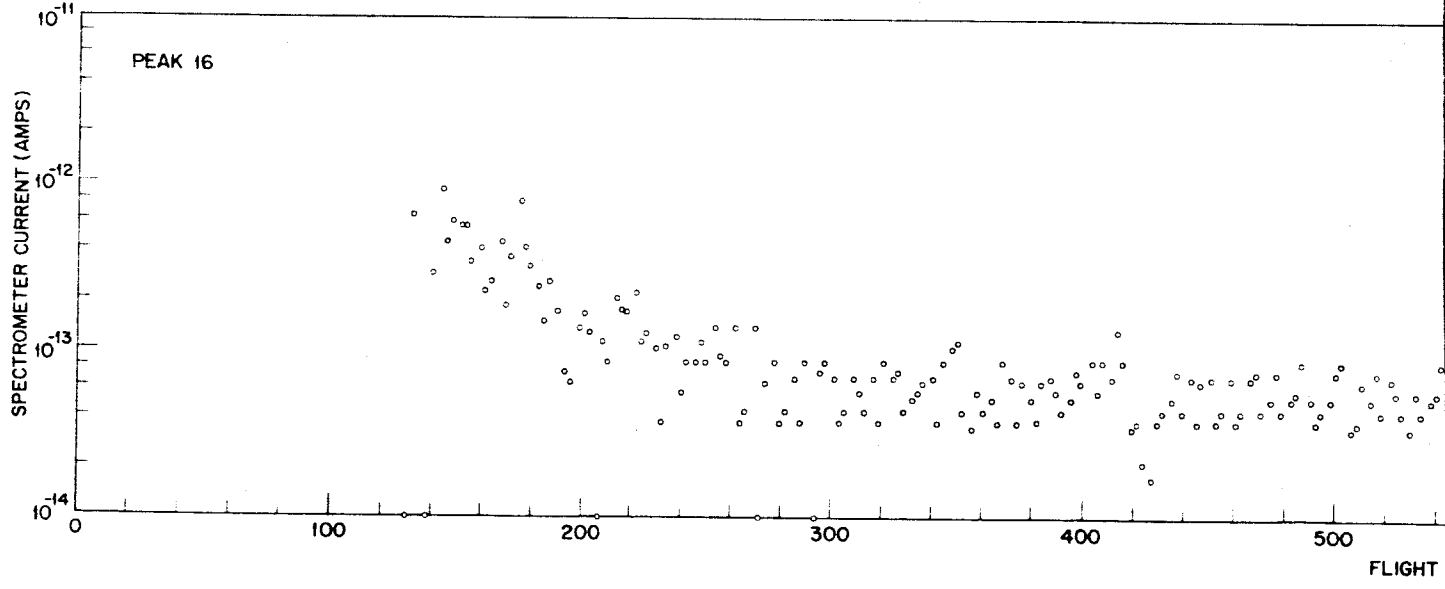
PEAK 16
SPECTROMETER CURRENT (AMPS)
$10^{-11}$
$10^{-12}$
$10^{-13}$
$10^{-14}$
0
100
200
300
400
500
FLIGHT

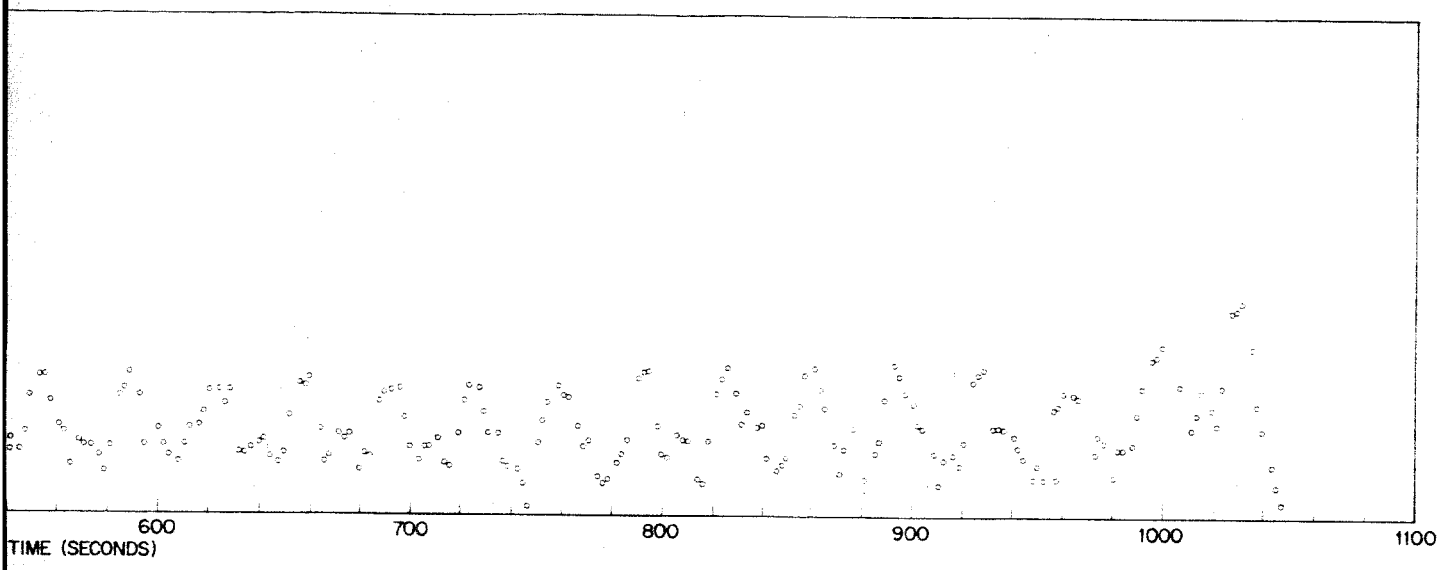
600
700
800
900
1000
1100
TIME (SECONDS)

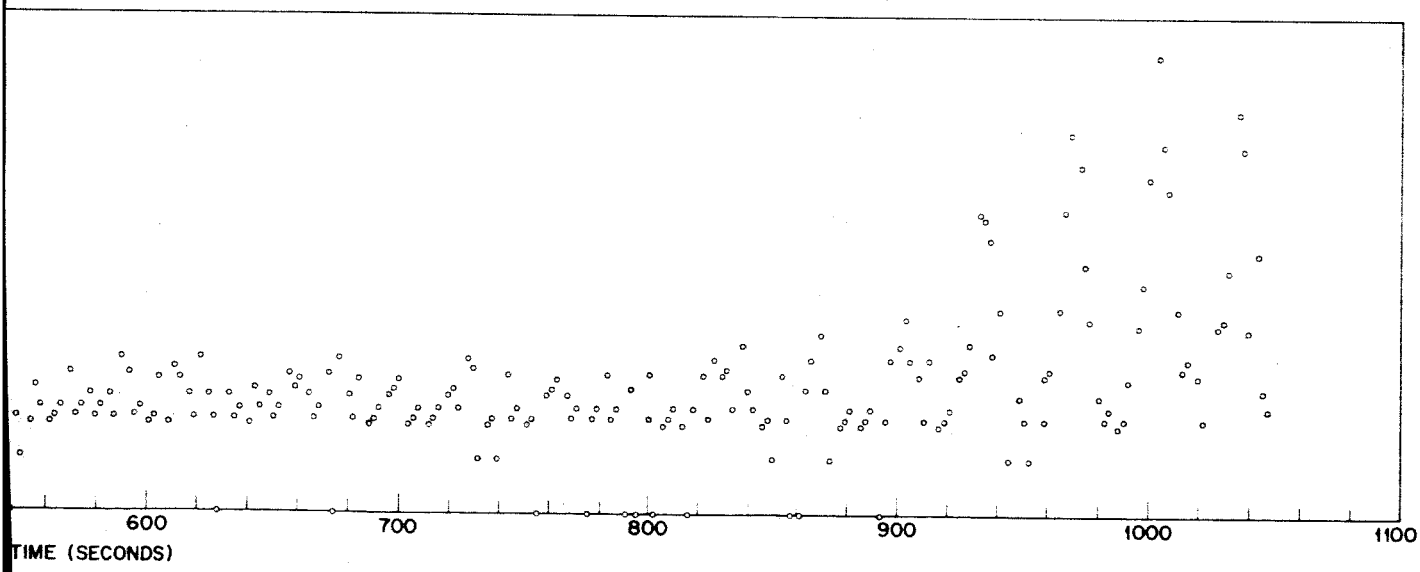
600
700
800
900
1000
1100
TIME (SECONDS)

Figure 17

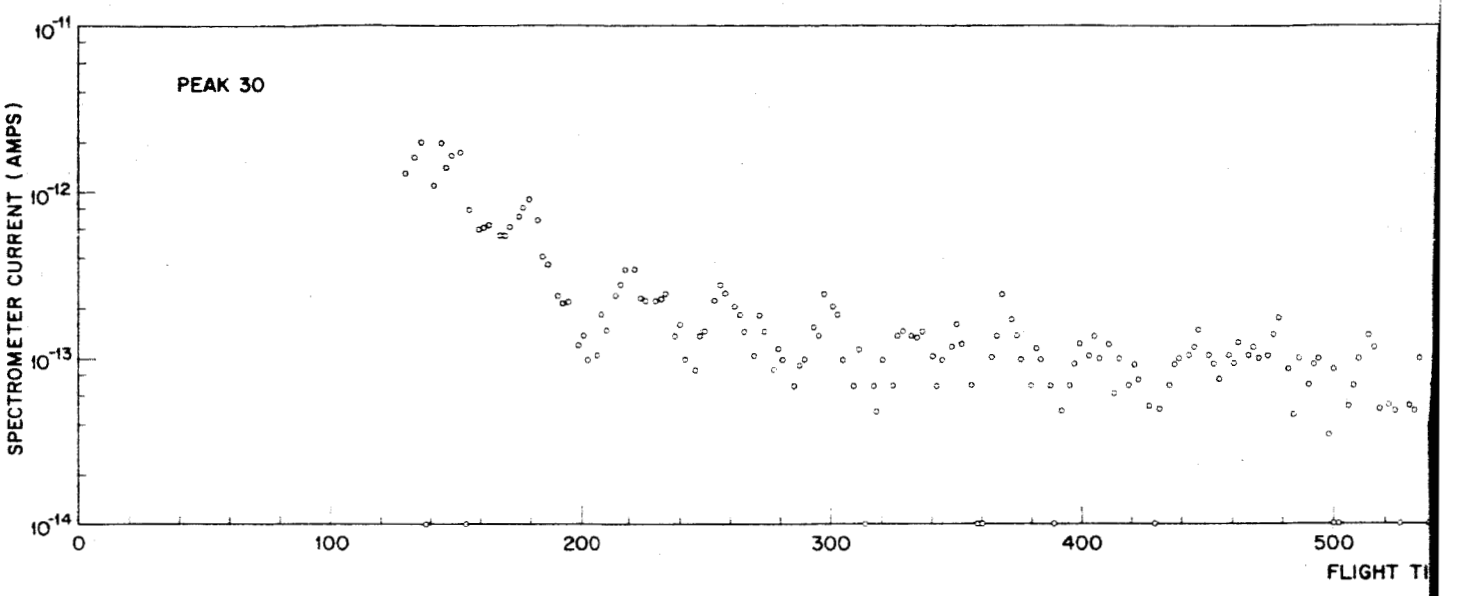
PEAK 30
SPECTROMETER CURRENT ( AMPS)
$10^{-11}$
$10^{-12}$
$10^{-13}$
$10^{-14}$
0
100
200
300
400
500
FLIGHT TI

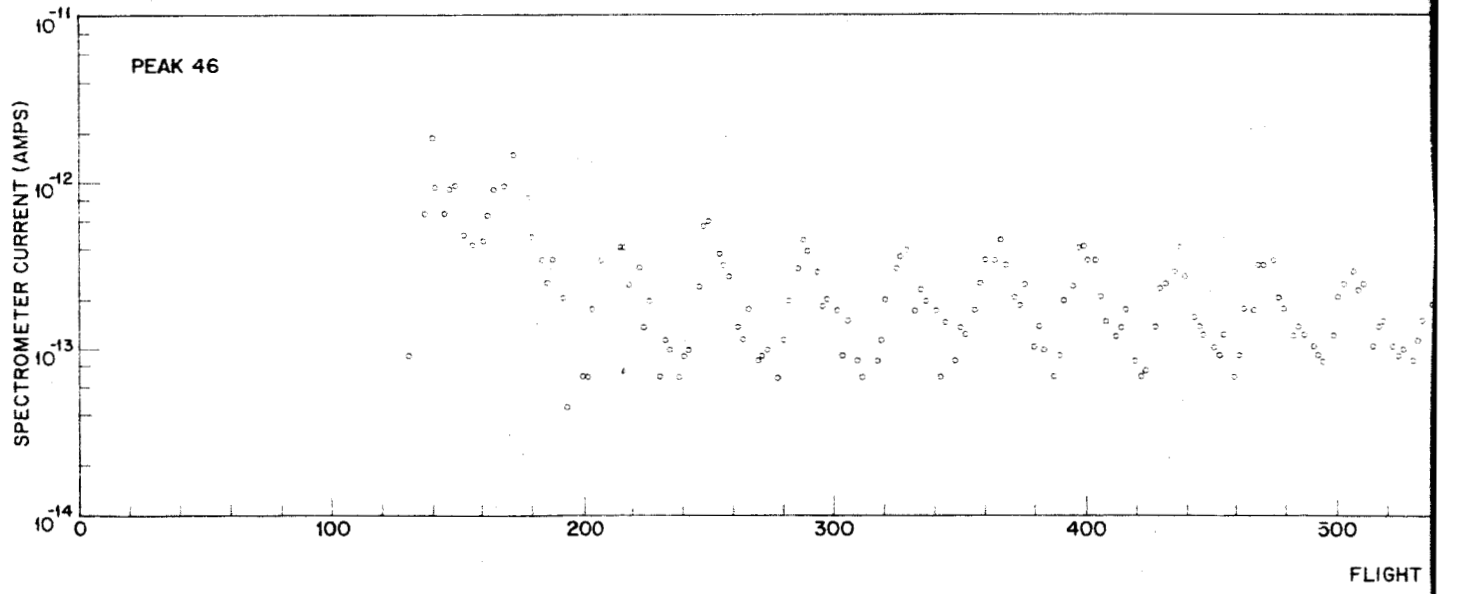
PEAK 46
SPECTROMETER CURRENT (AMPS)
$10^{-11}$
$10^{-12}$
$10^{-13}$
$10^{-14}$
0
100
200
300
400
500
FLIGHT

2

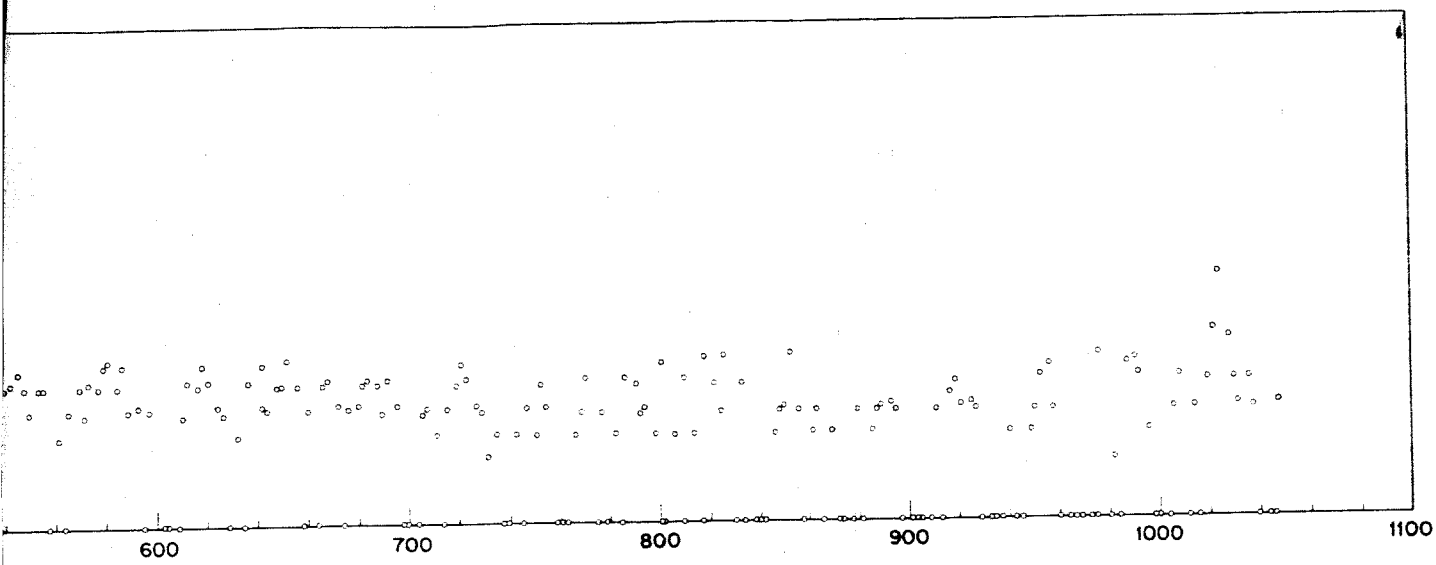


ME ( SECONDS )

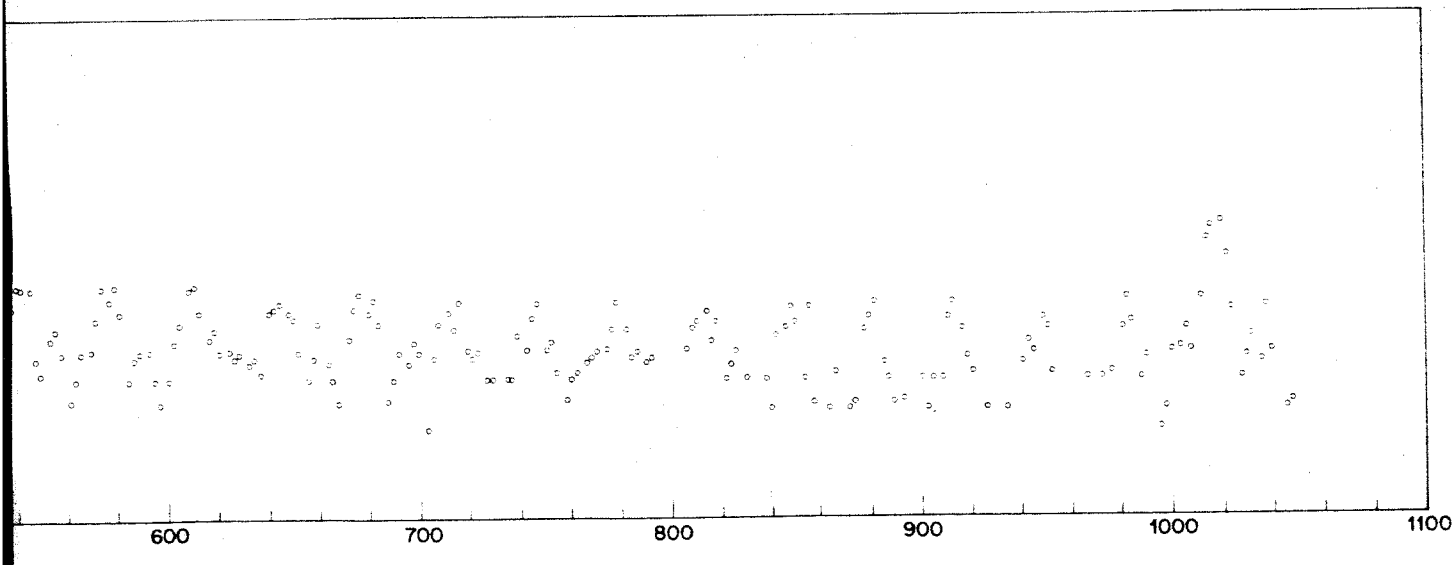


TIME (SECONDS)

Figure 18

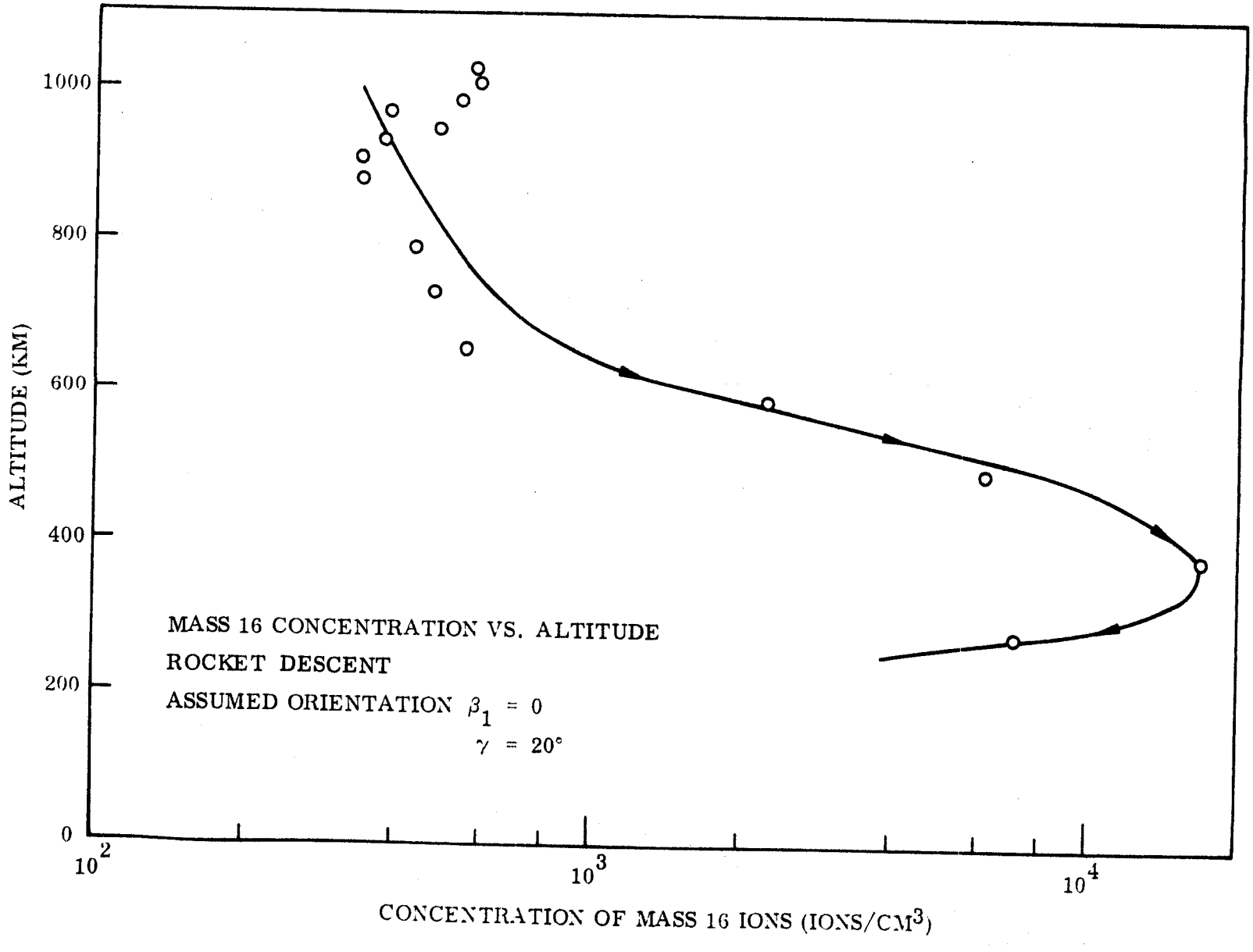
1000
800
600
400
200
0
ALTITUDE (KM)
MASS 16 CONCENTRATION VS. ALTITUDE
ROCKET DESCENT
ASSUMED ORIENTATION $\beta_1 = 0$
$\gamma = 20°$
$10^2$
$10^3$
$10^4$
CONCENTRATION OF MASS 16 IONS (IONS/CM$^3$)

Figure 19

## REFERENCES


Anderson, A. D., and W. E. Francis, A Semi-Theoretical Model for Atmospheric Properties from 90 to 10,000 km, Lockheed Missiles and Space Company, Rept. 6-74-64-19, 1964.

Bowen, P. J., R. L. F. Boyd, C. L. Henderson, and A. P. Willmore, Electron Temperature in the Upper F Region, Roy. Soc. London, Proc., 281A, 526-583, 1964A.

Bowen, P. J., R. L. F. Boyd, C. L. Henderson, and A. P. Willmore, Ion Composition of the Upper F-Region, Roy. Soc. London, Proc., 281A, 504-514, 1964B.

Brace, L. H., N. W. Spencer, and A. Dalgarno, Detailed Behavior of the Midlatitude Ionosphere from the Explorer XVII Satellite, Planet. Space. Sci., 13, 647-666, 1965.

Brubaker, W., "The Quadrupole Mass Filter" presented at IX Colloquium Spectroscopicum Internationale, Lyons, France, June, 1961.

Flowerday, T. W., "An Instrument for Measuring Ion Composition of the Upper Atmosphere," IEEE Trans. on Instrumentation and Measurement, Vol. IM-13, 14-16 March 1964.

Hanson, W. B., Satellite Environment Handbook, F. S. Johnson, Editor, Chapter 2, Stanford University Press, Stanford, California, 1961.

Hanson, W. B., Upper-Atmosphere Helium Ions, J. Geophys. Res., 67, 183-189, 1962.

Hanson, W. B., Electron Temperatures in the Upper Atmosphere, Space Res., 3, 282-302, 1963.

Hanson, W. B., and D. D. McKibben, An Ion-Trap Measurement of the Ion Concentration Profile Above the $F_2$ Peak, J. Geophys. Res., 66, 1667-1671, 1961.

Harris, I., and W. Priester, Theoretical Models for the Solar-Cycle Variation of the Upper Atmosphere, NASA Tech. Note NASA-TN D-1444, 1962.

Knudsen, W. C., and G. W. Sharp, Ion Concentration and Thermal Analysis of Data Obtained from an Ion Trap Carried in a Low-Altitude Rocket, oral presentation at conference on Direct Aeronomic Measurements in the Lower Ionosphere, Univ. of Illinois, Oct. 1963.

Knudsen, W. C., and G. W. Sharp, Evidence for Temperature Statification in the E-Region, J. Geophys. Res., 70, 143-160, 1965.

McWilliams, P., The Solution of the General Least Squares Problem with Special Reference to High-Speed Computers, Los Alamos Sci. Lab. Rept. LA-2367 Addenda, 1963.

Moore, R. H., and R. K. Zeigler, The Solution of the General Least Squares Problem with Special Reference to High-Speed Computers, Los Alamos Sci. Lab. Rept. LA-2367, 1960.

Nagy, A. F., and A. Z. Faruqui, Ionospheric Electron Density and Body Potential Measurements by a Cylindrical Langmuir Probe, J. Geophys. Res., 70, 4847-4858, 1965.

Nicolet, M., A Representation of the Terrestrial Atmosphere from 100 km to 3000 km, Penn. State Univ. Ionospheric Res. Sci. Rept., 155, 1962.

Paul, W., H. P. Reinhard, and U. Von Zahn, Z. Phys., Vol. 152, p. 143, 1958.

Pearse, C. A., A Method for the Measurement of Ionic Density, Temperature and Composition at High Altitudes, in Electron Density Profiles in the Ionosphere and Exosphere, edited by B. Maehlum, pp. 194-203, MacMillam Company, New York, 1962.